Accommodation of compression and lateral extension in a continental crust: Analogical modeling of the Central Atlas (eastern Algeria, Tunisia) and Pelagian sea

Rabeb Dhifaoui, Pierre Strzerzynski, Régis Mourgues, Adel Rigane, Claude Gourmelen, David Peigné

TITLE:

Accommodation of compression and lateral extension in a continental crust: Analogical modeling of the Central Atlas (eastern Algeria, Tunisia) and Pelagian sea.

Author names and affiliations:

***Rabeb* Dhifaoui[(1, 2)], *Pierre* Strzerzynski[(2)], *Régis* Mourgues[(2)], *Adel* Rigane[(1)], *Claude* Gourmelen[(3)], *David* Peigné[(2)]**

1 Université de Sfax, Faculté des Sciences de Sfax, Laboratoire "GEOMODEL - LR16ES17. BP. 1171 Sfax 3000 - Tunisie
2 Laboratoire de Planétologie et de Géodynamique, CNRS, Le Mans Université, Le Mans, France
3 Université du Maine, Faculté des Sciences, Laboratoire de Géosciences, Av. O. Messiaen, F 72085 Le Mans cedex 9, France

Corresponding author:
Pierre Strzerzynski
Pierre.strzerzynski@univ-lemans.fr

Abstract:

At the eastern boundary of the North African Alpine Chain (NAAC), coexisting grabens, thrusts, and strike-slip faults form a complex structural pattern in the general context of Nubia-Eurasia plates convergence. In a context where the root of several major structures is poorly constrained, debates exist on the possible roles of orthogonal to shortening extension, décollement layer at the base of the Mesozoic cover, and lithospheric scale processes such as delamination. We present analog modeling experiments of shortening and/or orthogonal extension applied to an upper-crust consisting of sand lying on weighted silicon. When considered, a second silicon layer mimics a décollement at the basement-cover boundary.

Our results highlight: 1) The regional structural pattern results from both crustal shortenings related to convergence between Nubia and Eurasia plates and orthogonal extensions due to a far-field pull of the Western-Hellenic/Dinaride subduction. 2) Several large-scale structures such as the Zaghouan thrust faults, the Sicilia Channel rift system, and the Gafsa Fault zone root deep into the continental crust. 3) The Atlas Triassic décollement layer is responsible for thin-skin tectonics in the Atlassic domain leading to the formation of surface folds called "Djebels", extension in the "Fossés" area, and also favoring underplating of upper-crust slices in northern Tunisia. 4) Misfit on dominating extension direction at the wedge top between model and nature highlights the role of processes at the scale of the lithosphere such as the formation of a crustal root below the Atlassic wedge and opposite vertical motions between Atlas and Pelagian areas as a consequence of lithospheric delamination.

Keywords:

Analog modeling, Pelagian Sea, Tunisian Atlas, thin-skin tectonics.

1. Introduction

In Mediterranean Regions, the complex orogenic pattern is the result of lithospheric slab dynamic and back-arc basin opening (Carminati et al., 1998, Jolivet and Faccenna 2000, Faccenna et al., 2004, van Hinsbergen et al., 2014). The curved shape of convergence zones located around the Western Mediterranean sea can be explained by the fragmentation (Huw Davies and von Blanckenburg, 1995, Lonergan and white 1997) and the segmentation (Faccenna et al., 2004, Wortel et al., 2009, Gutscher et al., 2017, Ficthner and Villaseñor, 2015) of the Tethysian slabs prior or during slabs roll-back (fig. 1). These result in very contrasted orogenic evolution stages from active oceanic subduction processes in the Alboran and Calabrian areas (Lonergan and white 1997) to collision post dating a slab break-off event and coeval with peeling in the North African Alpine Chain (NAAC) (Maury et al., 2000, Roure et al., 2012, Booth-Rea et al., 2018).

NAAC underlines, over 2000 km, the east-west boundary between the Africa plate and the western Mediterranean basin and forms the most important reliefs of Southern Spain, Morocco, Algeria and, Tunisia (fig. 1). It is bounded to the north by the Algerian basin consisting of Cenozoic oceanic crust (Dewey et al., 1989; Carminati et al., 1998, van Hinsbergen et al., 2014). At the western boundary of the NAAC, the Rif-Tell-Atlas system in Morocco underlines the transition between post-collisional to still-subducting systems. To the east, NAAC is prolonged by a large submerged continental plateau called the Pelagian sea and then the Ionian Sea that consists of a Mesozoic oceanic domain plunging

bellow the Eurasia plate in the Calabrian and Mediterranean ridge subduction zones (fig. 1). The transition here takes place in an emerged-submerged domain where orogenic processes compete with extension. This results in a complex tectonics context characterized by coeval shortening, strike-slip, and, extension in an area covering the East of Algeria, Tunisia and, the Pelagian marine domain (fig. 1: Martinez et al., 1985, Philip et al., 1986, Rabaute and Chamot-Rooke, 2014).

Several studies have successfully applied analog model approaches to the tectonics matters of the NAAC eastern boundary (Corti et al., 2006, Sokoutis et al., 2011, Belguith et al., 2013, Khelil et al., 2019, Fedorik et al., 2018) and neighboring areas (Henriquet et al., 2020, Strzerzynski et al., 2021). Some focus on the shortening/extension interplays (Corti et al., 2006, Khelil et al., 2019) whereas others explore the shortening/strike-slip relationships (Sokoutis et al., 2011, Fedorik et al., 2018). In experiments considering only an extension, Belguith et al. (2013) highlight the importance of a décollement layer on the position and the size of grabens both in the Pelagian domain and in Tunisia. Considering these results, initial experimental conditions that can reproduce the eastern NAAC structural pattern, have not already been found.

The objective of the study, we follow an analog modeling approach to replace the eastern termination of NAAC association of structures in a broader geological context. Better constraints especially on the role of Triassic salt, on the root of major structure, and the origin of the lateral extension, are awaited. For this, we successively explore the influence of lateral extension and ductile décollement layer on an ongoing brittle sand wedge simulating the brittle crust.

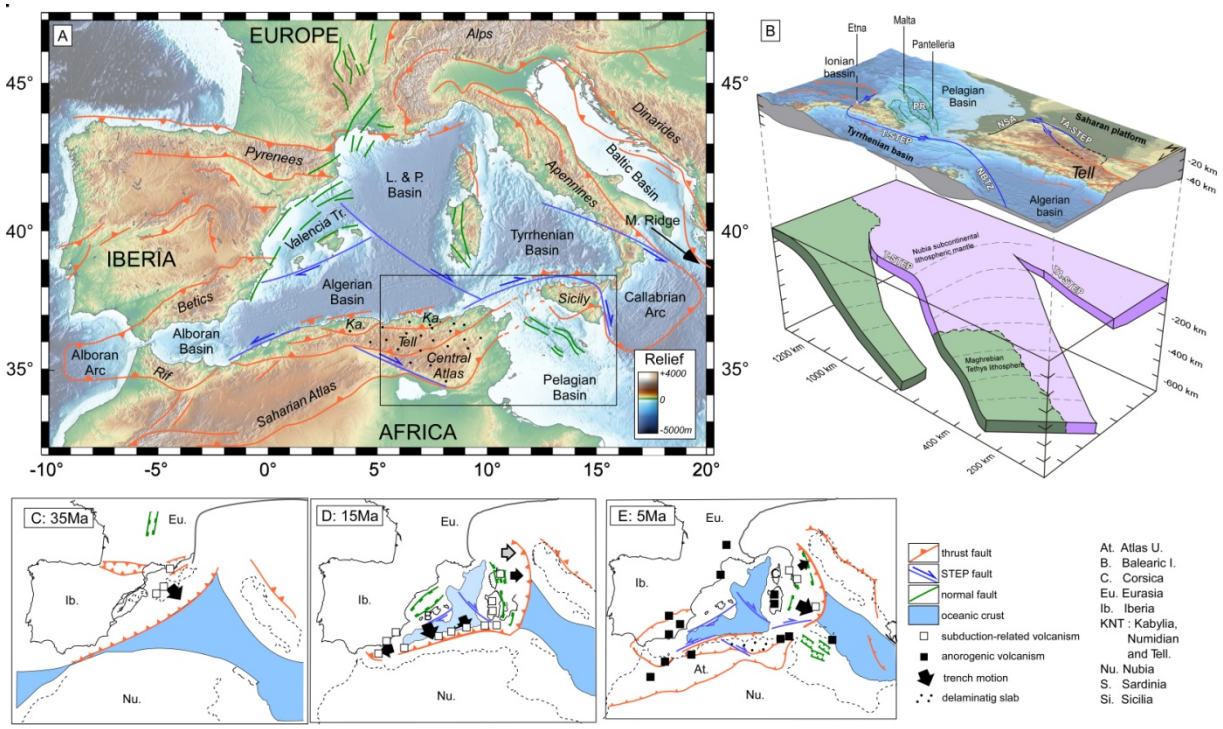

Figure 1: The Algerian and Tunisian Atlas unit in the context of the western Mediterranean area. A: structural map of the Western Mediterranean domain plotted on SRTM 30' DEM. Tectonic structures are modified after Billi et al., 2011, van Hinsbergen et al., 2014, Fichtner and Villasenior, 2015, Booth-Rea et al., 2018. black rectangle: the position of Figure 2, 3 maps. B: Tectonic sketch of the mantle structure under the Calabrian and Tunisian arcs (modified after Booth-Rea et al.,

2018), C: Reconstruction of the evolution of the Mediterranean region in relative (Eurasia fixed) reference frame in three stages, from 35 Ma to present-day (modified after Faccenna et al., 2004 and van Hinsbergen et al., 2014.

2. Geological context

The NAAC is an example of oceanic subduction to continental collision orogenic belt where Rif-Kabylie, Numidian, Tell and Atlas units represent respectively the internal part, the suture zone, the Tethyan passive margin, and the stable continental domain (fig. 2; Wildi 1983). The northern position of the internal unit is compatible with a subducting slab dipping to the north as observed further to the East in the Calabrian subduction zones. Ophiolites and high-pressure low-temperature metamorphism are missing as well as tomographic evidence of subducted lithosphere connected to the suture zone (Carminati et al., 1998, van Hinsbergen et al., 2014). Such an absence has been interpreted as a slab break-off that may have occurred during the early stage of collision. This scenario is supported by chemical changes on Miocene volcanic rocks from the internal and Tell units (Maury et al., 2000), evidence of extension tectonic (Aite and Gélard, 1997, Booth-Rea et al., 2018) and, the back-arc position of the Western Mediterranean basin (Dewey et al., 1989; Carminati et al., 1998, van Hinsbergen et al., 2014). Models of subduction transform edge propagator (STEP faults) are proposed to explain the peculiar geometry of slab that is detached to the west and still subducting to the east (fig. 1; Wortel et al., 2009, Gutscher et al., 2017). Below the NAAC, a high-velocity anomaly located 200 km has been interpreted as a peeling of the African lithospheric mantle that may have facilitated the stain transfers to the southern boundary of the belt in Tunisia (Roure et al., 2012, Fichtner and Villasenior, 2015, Booth-Rea et al., 2018).

Convergence rates are low, velocities ranging between 5 and 10mm.yr-1 and decreasing (Fig. 3; Dewey et al., 1990, Rosenbaum et al., 2004). Present-day velocities along the Eurasia–Africa Plate boundary at the Tunisian longitudes are 7 $mm.yr^{-1}$ along an N150° direction as estimated by geologic methods (Argus et al., 2011; Demets et al., 2015) and around 5 $mm.yr^{-1}$ along an N130° when using geodetic methods (fig. 3; Calais et al., 2003; Serpelloni et al., 2007, Altamimi et al., 2017, Bougrine et al., 2019, Bahrouni et al., 2020).

Our studied area (fig. 2) is located at the eastern termination of the NAAC and concerns the north-east of Algeria, Tunisia, and a part of the Pelagian domain. It is a 450*450km large area bounded by the Western Mediterranean basin to the north, the Ionian Sea to the East, and the Saharian desert to the south. Kabylie, Numidian flysch and Tell units are localized on a 50 km large area bounding the western Mediterranean basin shoreline, and the rest of the studied area is occupied by the Atlas units and the Pelagian domain (Wildi 1983).

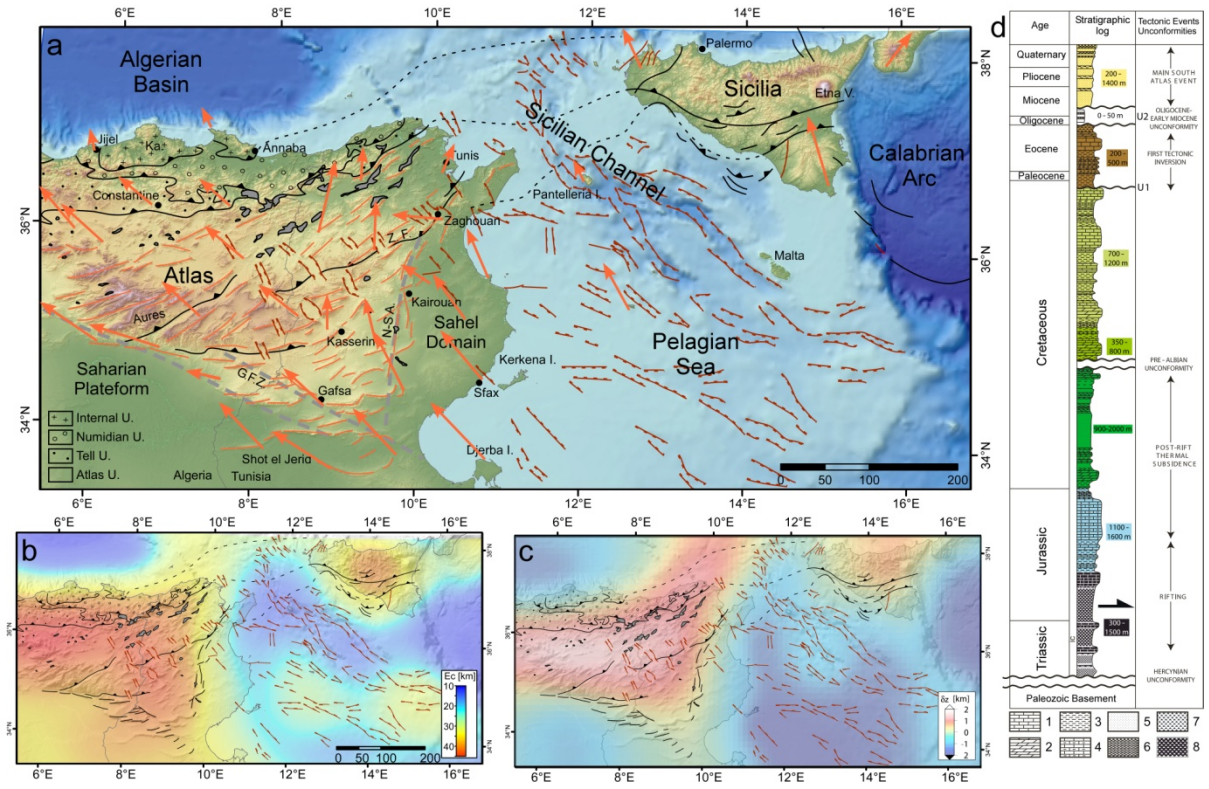

Figure 2: a) Structural map of the region between eastern Algeria, northern Tunisia, and Sicily displaying main tectonics units. Black, red and, orange lines are thrusts, normal faults, and anticlines. Grey areas are salt diapirs, G.F.Z.: Gafsa fault zone, N-S A.: Nord-south axis, Z.F.: Zaghouan fault, Ka.: Petite Kabylie. b) Crust thickness (after Globig et al., 2016) and c) residual topography (after Boschi et al., 2010), d) stratigraphic log of the Mesozoic-present cover (after Said et al., 2011) 1) Limestone, 2) Dolomite, 3) Clay, 4) Marl, 5) Sand, 6) Conglomerate, 7 & 8) Evaporites

3. Geological evolution of NAAC

The Geological formations of the eastern termination of the NAAC consist of Triassic to present sedimentary cover deposited on a continental crust. During the Mesozoic, depositions occurred in a context of extension. It begins with the formation of a Triassic basin filled with evaporite deposits across most of Tunisia (fig. 3D; Kamoun et al., 2001). Triassic rocks consist of gypsum and halite, interbedded with clays and dolomites (Laaridhi-Ouazâa, 1994). They are covered by Jurassic carbonates that represent the Maghrebian Tethys syn-rift deposits on the whole of Tunisia (Soussi, 2000; Boughdiri et al., 2007). During the Early Cretaceous, platform environments dominate the central and southern part of the studied area (Gharbi et al., 2013) whereas strong subsidence and NW-SE directed extension lead to the formation of a trough to the North (Souquet et al., 1997). Then, the whole studied area records a Late Cretaceous to Eocene post-rift sedimentation dynamics characterized by the cyclic changeover of shallow marine carbonate and open marine shale deposition (fig. 2D).

The North oceanic subduction of the Tethyan domain below the internal unit starts probably during the Cretaceous. Internal units are assumed to belong to Iberia during Eocene time during an early stage, (Roca et al., 2001). Then, it separates from Iberia during the Oligocene, leading the Western Mediterranean basin to open in a back-arc position (fig. 1C). At that time, deformation affects mostly the Numidian flysch nappe (fig. 2A; Carminati et al., 1998, Roure et al., 2012, van Hinsbergen et al.,

2014). In the central part of the NAAC, the collision between the internal unit and Africa plate passive margin occurred at the end of the early Miocene (fig. 1D). It is associated with tectonics within the Tell unit (Fig. 2), ending of the back-arc opening, and at depth, to slab break-off. During the late Miocene, deformations propagate southward and affect the Atlas unit. Since the Pliocene (fig. 1E), deformations are shifting northward from the Atlas unit to the southern boundary of the Internal unit (Boudiaf et al., 1999) and also to the Algerian margin (fig. 1A; Deverchère et al., 2005, Domzig et al., 2006, Strzerzynski et al., 2010).

Two major shortening events take place between Late Cretaceous to Present. First, a mid to late Eocene contractional event (Bouaziz et al., 2002, Masrouhi et al., 2014; Frizon de Lamotte et al., 2009; Melki et al., 2011, Khomsi et al., 2009) causes the inversion of Mesozoic basins. It is followed by a major orogenic episode characterized by northwest-trending shortening leading to the formation of a fold-and-thrust belt from northwest to southeast (Martinez and Truillet, 1985, Chihi and Philip, 1998). Thus, the studied area shows a complex tectonic organization, structured mainly since the Late Miocene, combining thrust, strike-slip, and normal faults (Martinez et al., 1985, Chihi and Philip, 1998) (fig. 2A). We distinguish three domains on the Atlas units and the Pelagian domain that are from East to West (fig. 2A and 3): the eastern domain affected mostly by extension, the central Atlas where the shortening is the most expressed, and the Saharan Atlas where deformations are absent.

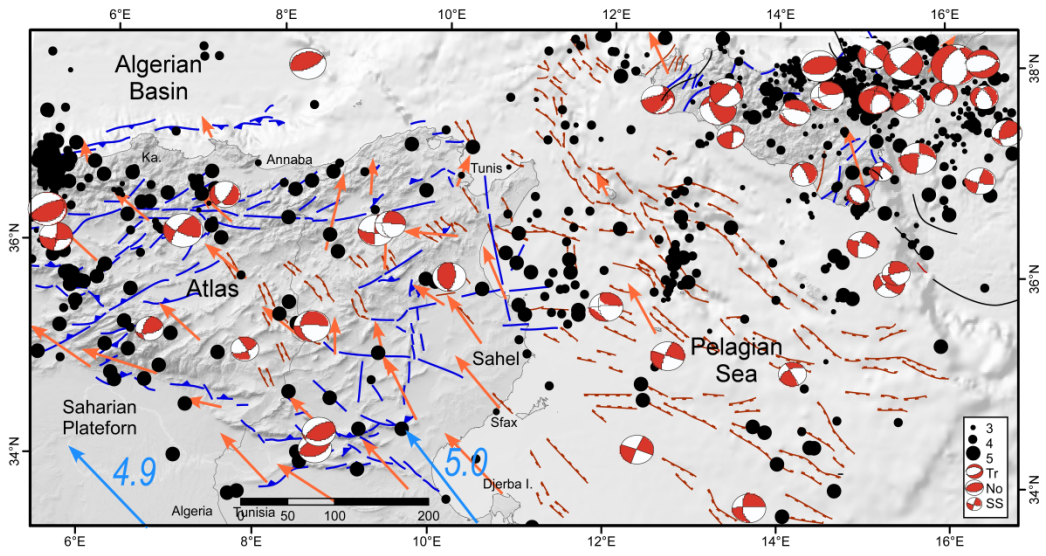

Figure 3: Structural map of the region between east Algeria, northern Tunisia, and Sicily displaying available geodetic data, earthquake position, focal mechanisms, and present-day actives structures. Orange and blue arrows are GPS velocities relative to Eurasia taken from Bahrouni et al. (2020) and Nubia and Eurasia plates convergence after Nuvel-1A (DeMets et al. 1994). The structural framework is from Rabaute et al., 2014, in blue: reverse and strike-slip faults and in red: normal faults. Black dots are the instrumental seismicity from CMT USGS-Harvard. Focal mechanisms are from Serpelloni et al., 2007. No: normal, faulting, Tr: thrust faulting, SS: strike-slip faulting

3.1. Geology of Saharian and Eastern units

In the Saharian unit, continental crust and lithosphere are 25-30 km and 80 km thick, respectively (fig. 2B). In addition to these usual crustal and lithospheric thicknesses, the absence of significant earthquakes in this area suggests a stable continental domain (fig. 3). Very low topography of the

Chott basin and negative residual topography (fig. 2C; Boschi et al., 2010) are in good agreement with possible subsidence in this area.

The Eastern domain is a marine and continental domain composed of an emerged area located to the East of the N-S axis and called the Tunisian Sahel and the Pelagian domain (fig. 2A). Onshore, Tunisian Sahel reliefs are low, and offshore, the bathymetry of the Pelagian sea consists of a submerged continental plateau with a mean bathymetry of -100 m (fig. 2A). Between Sicily and Tunisia, bathymetry strongly decreases down to -1700 m within NW-SE elongated trough bounded by the volcanic island of Pantelleria, Linosa, and Malta (fig. 1A and 2A). Mean absence of relief, negative residual topography anomaly (fig 2c; Boschi et al., 2010), and sedimentation rate (Patriat et al., 2003) suggests subsidence starts during the Miocene and is still active today (Khomsi et al., 2004, Ben Brahim et al., 2013, 2014, Arab et al., 2020). Crustal thickness is less than 30 kilometers and decreases progressively from West to East below the Tunisian Sahel (fig. 2b). It reaches minimum values around 15 kilometers below Malta, Pantelleria, and Linosa troughs (fig. 2b). In the Pelagian domain, NW-SE elongated trough, volcanic activity (Civile et al., 2008), high heat flow, thin continental lithosphere (Jiménez-Munt et al., 2003), and seismicity are compatible with crustal thinning processes (Fig. 3; Catalano et al., 1995). NW-SE extension direction is evidenced by geodetic data evidencing also a sinistral strike-slip component of the motion between Sicilia and Tunisia (Serpelloni et al., 2007, Bahrouni et al., 2020). Here, the extension starts during the late Miocene (Argnani 1990, Civile et al., 2008, Arab et al., 2020). It affects the whole Pelagian zone as normal NNO-SSE oriented faults forming the boundaries of Malta, Pantelleria, and Linosa grabens (fig. 2a; Argnani 1990, Civile et al., 2008). On the Pelagian plateau and below the Tunisian Sahel, the extension is also well expressed with the formation of graben full filled by Upper Messinian to present deposits that predate shortening (fig. 2A; Khomsi et al., 2004, Ben Brahim et al., 2013, 2014, Arab et al., 2020). The relative timing of magmatism and tectonics suggests that extension here can be referred to as a 'passive' rifting model (Civile et al., 2008). The size and amplitude of grabens suggest that Malta, Pantelleria, and Linosa grabens are influenced by the basement. Such an extension has also been recognized in seismic lines under the Sahel and in the North Atlas domain where they overprint the compressive structures (fig. 2A). The sizes and frequencies of these structures suggest that extension roots at the basement/cover boundary (Belguith et al., 2011).

3.2. Geology of Central Atlas

The highest reliefs are founded in the **central Atlas** unit where they follow an N50 trend slowly decreasing from the Aures mountains to the Cap Bon (fig. 2A). To the northwest, altitudes stay relatively high up to the coastal domain where 1000m high hills of the Petite Kabylie plunge directly into the Western Mediterranean basin. To the Southeast, relief decreases more progressively (fig. 2A). Over thickened crust consist of a triangular-shaped area located below the central atlas (fig. 2 and 3, Rigane and Gourmelen, 2011)). In the Western Mediterranean basin, crustal thickness decrease strongly and reach less than 10 km at the oceanic-continent transition (fig. 2B), as a consequence of slab break-off (Carminati et al., 1998, van Hinsbergen et al., 2014, Chertova et al., 2014). Residual positive topographies (fig. 2c; Boschi et al., 2010) suggest that uplift is still active.

In the northern half of the Central Atlas unit, the deformation consists of a set of folds and faults (Zouaghi et al., 2011) (fig. 2a). Triassic evaporites are common at the outcrop and have given part of this area the term "diapir zone" (fig. 2a). This area is characterized by the most important reliefs and

the thickest continental crust suggesting that deformation affects not only the sedimentary cover but also the upper crust (fig. 2). Such a deep tectonic has been proposed at the Tellian-Atlas boundary by wide-angle seismic profile ("The EGT'85 seismic experiment in Tunisia: a reconnaissance of the deep structures," 1992) and further south all along the Zaghouan fault and a fault system bounding the Aures mountain (fig. 2A; Morgan et al., 1998, Khomsi et al., 2016, Bahrouni et al., 2020). Towards the South, crossing the central Atlas, the deformation gradually lose intensity, and the relief decreases (fig. 2). Deformation is characterized by kilometer-scale anticlines and folding the sedimentary series and called djebels (fig. 2) (Outani et al., 1995, Saïd et al., 2011, Ahmadi et al., 2013, Haji et al., 2014).

An extension is also described on the northern half of the Central Atlas unit (fig. 2a; Burollet, 1956, Caire et al., 1977). It consists of several kilometer-long grabens with an NW-SE strike direction (Belguith et al., 2011, Bahrouni et al., 2014). Normal faults are cutting previously formed compressive structures suggesting that these were active since the latest Miocene (Belguith et al., 2011, Bahrouni et al., 2014). Geodetic results in this area indicate that extension is still active today (fig. 3; Bahrouni et al., 2020). Experimental results on the formation of grabens from the Central Atlas unit (Belguith et al., 2011) highlight that grabens root into the Triassic evaporite décollement level and do not affect the continental crust. Such a result is in good agreement with the limited seismic activity and especially the absence of focal solution compatible with NE-SW direction of extension (fig. 3; Rabaute and Chamot-Rooke, 2014, Soumaya et al., 2015).

Boundaries between the Central Atlas and the Saharian platform, to the West and the Eastern domain to the East, are called the Gafsa fault zone and the N-S axis respectively (fig. 2a; Zargouni,1985, Zouaghi et al,2005, Rigane and Gourmelen, 2011). Moderate seismicity is present along with these structures and is characterized by strike-slip to reverse focal mechanisms (Rabaute and Chamot-Rooke, 2014, Soumaya et al., 2015). Geodetic data confirm the present-day motion of the Gafsa fault zone and document a 1.5 mm.yr-1 dextral strike-slip motion (Bougrine et al., 2019, Bahrouni et al., 2020) whereas evidence for a present-day activity of the N-S axis is ambiguous. On the surface, the Gafsa fault zone and the N-S axis consist of areas where numerous Djebels display dispersed trends (Zouaghi et al,2005, Rigane and Gourmelen, 2011). A sinistral component is inferred for the N-S axis from geological evidences (Rigane and Gourmelen, 2011). Gafsa fault zone and N-S axis are interpreted as the surface expression of lateral (STEP fault; Govers et al., 2005) and frontal boundaries of the delaminated mantle slab (Fig. 1B; Booth-Rea et al., 2018).

4. Experimental procedure

1.1.Experimental setup and monitoring

We adopt a classical method of analog modeling, following the work of Belguith et al, 2013. The experiments consist of a crustal brittle-ductile PVC box subjected to shortening and orthogonal extension as two lateral borders/backstops are mobile-driven by motorized worm screw at constant displacement rates (fig. 4). The compression simulates the convergence between the Eurasian and African Plates and the extension represents a free edge located at the level of the Mediterranean ridge.

Monitoring of the experiment is provided by three digital cameras shooting the model surface with different tilts every 5 min. The spatial resolution of images is around 0.15 mm/pixel and the maximum displacement between two pictures around 0.4 mm.

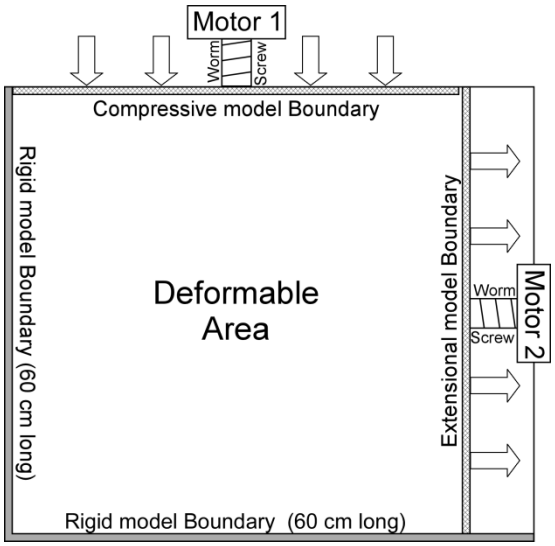

Figure 4: Upper view of the experimental setup consisting of a deformation device and CCD cameras (not represented)

Post-processing of the experiment consists of time-lapse video building, displacements/deformation measurements, and Digital Elevation Model (DEM) acquisitions. Horizontal surface displacements and deformations are quantified using Particle Imaging Velocimetry (PIV) technique based on optical image correlations (White et al.,2003; Adam et al., 2005). As demonstrated by White et al. (2001), PIV cross-correlation allows the calculation of displacements with sub-pixel accuracy (0.1–0.2 pixel). In our case, as the maximum displacement is about 4 pixels between two pictures, such a technique allow us to determine significant displacement down to 0.01 mm. Surface topography models are obtained by stereo-photogrammetry using tree simultaneous pictures and the Agisoft Photoscan© photogrammetric processing software. Such an approach has been successfully applied to analog experiments (Lelandais et al., 2016) and can provide a topographic grid with a resolution of 0.5 mm and a vertical precision of 1 mm.

Internal model Structures and deformations are investigated only for the final stage of each experiment by removing successively each sand and silicon layers and taking pictures after each removal. To better record the finite deformation, we dust a thin layer of blue sand on a grid during the filling of each experiment.

Our models are made of alternating layers of brittle and ductile materials. The upper crust is simulated by two layers of dry sand of Fontainebleau and an intermediate ductile layer of silicone putty (SGM 34), corresponding to the Triassic evaporites (Table 1). Several experiments were carried out by changing two parameters: 1) the number of model layers and the motion applied on model edges (Fig. 4 and 5). 2-layers experiments (M1 and M2) simulate the upper crust deformation as a unique brittle layer lying on a ductile lower crust whereas 4-layers experiments take into account the occurrence of a 5 mm sedimentary cover separated from the basement by a 5 mm ductile evaporite layer. M1, M2, M3, and M4 are subjected to shortening and additional orthogonal extension is applied only in the case of the M3 and M4 experiment. Extension without shortening is applied to a 4

layers model on M0 to compare our result with those of Belguith et al., 2013. For each experiment, the displacement velocity 5 mm.h^{-1}, and the duration is about 20 hours (Fig. 5).

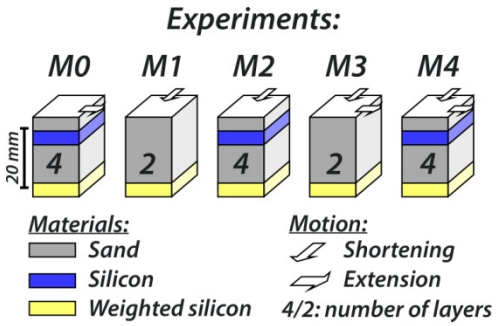

Figure 5: initial condition (number of layers) and deformation (motion) applied on the 5 presented experiments.

1.2.Scaling and experimental parameters

As stated by Hubbert (1937) and Ramberg (1981), analog modeling requires geometric and dynamic similarities between nature and the prototype. Applied to geodynamics, the method consists of 1- calculating vertical strength profiles for the natural example and its prototype made with brittle (frictional) and ductile (viscous) materials and 2- subjecting the model to gravity and tectonic deformation (Davy and Cobbold, 1988, 1991).

The main parameters controlling the rheological profile of the natural crust are rocks petrology, heat flux, Moho depth, and deformation rate. To respect the similarity between the natural and experimental models, the dimensions and stresses must conform to the equation of dynamic equilibrium:

$\sigma^* = \rho^* . g^* . L^*$ (eq.1)

where σ is the stress, ρ the density, g the acceleration of gravity, L the length, * Indicated model/nature ratios. Experiments are carried out under normal gravity so that g*=1. L* is set to 1.3 10^{-6}, this means that the 60*60 cm area covered by the model corresponds to a square of about 500 km side in the nature. Considering volumetric masses of 2600 kg.m^{-3}, 2500 kg.m^{-3}, and 2700 kg.m^{-3} for natural sedimentary rocks, evaporites and the continental crust, respectively, the average scaling ratio for volumetric mass (ρ*) is 0.5. Based on these values, the resulting stress ratio σ* is 8.0 10^{-7}.

In the upper crust, the majority of materials deform in a brittle manner according to the equation of Mohr-Coulomb:

$\tau = \sigma_n . \tan\phi + c$ (eq.2)

where: τ is the shear stress, σ_n, The normal stress, ϕ, the angle of internal friction, and c the material cohesion. The analog material must follow the same rheological law with cohesion C respecting the

stress ratio σ*. The Fontainebleau dry sand has a negligible cohesion (Co < 50 Pa) and a friction angle equal to 30° (Lelandais et al., 2016; Strzerzynski et al., 2021).

For the viscous layers of the crust (lower crust and ductile rocks as evaporites) the physicals parameters must respect the following ratios:

$$\sigma^* = \mu^* . \acute{\varepsilon}^* \quad \text{(eq.3)}$$

$$\acute{\varepsilon}^* = 1/t^* \quad \text{(eq.4)}$$

where μ* is the viscosity ratio, and έ* the deformation rate ratio. Long lasting salt tectonics processes within Tunisian Triassic evaporite lead in an absence of a continuous rock-salt layer (Kamoun et al., 2001). Considering this, we used an average dynamic viscosity for evaporite of 1×10^{20} Pa.s based on anhydrite viscosity (e.g. Chemia et al., 2009, Burchardt et al., 2012) rather than Rock-salt. This yields a model/nature ratio for viscosity η* of $2*10^{-16}$.

As the silicones used to simulate the evaporites and the lower crust don't have a sufficiently strong viscosity contrast, we do not try to simulate deformations of the lower crust. The lower crust is replaced by a thin layer (5 mm) of weighted silicon playing the role of a décollement layer (the silicon is weighed down by the addition of barite to respect the density ratio). The small thickness of the basal layer is chosen to artificially increase the shear strength of the weighted silicon. Nevertheless, by artificially replacing the lower crust with a basal thin viscous décollement layer, our models have some difficulties simulating correctly isostatic balancing at crustal scale.

Parameters		Model	Nature	Model/Nature
Length (m)				
	Horizontal distances	0.6000	400000	1.50E-06
	Sediment thickness	0.0060	4500	1.33E-06
	Evaporite thickness	0.0045	1000	4.50E-06
	Upper Crust thickness	0.0120	10000	1.20E-06
Density ($Kg.m^{-3}$)				
	Sediment	1500	2700	0.56
	Evaporite	1000	2500	0.40
	Upper Crust	1500	2700	0.56
	basal	1650	2700	0.61
Viscosity (Pa.s)				
	Evaporite	2.00E+04	1.00E+20	2.00E-16
	basal décollement	6.00E+04	5.00E+20	1.20E-16
Gravity acceleration (m/s^2)		9.81	9.81	1.00
Time (s)	*aka durations*	7.20E+04	3.16E+14	2.28E-10
Speed ($m.s^{-1}$)	aka short./duration	1.39E-06	2.11E-10	6.57E+03

Table 1 : Model scaling parameters: comparison between model and nature.

Strain rate calculation after eq. 3 yields to $\acute{\varepsilon}^* = 4.0 \times 10^{9}$, from which a model/nature time ratio can be quantified. As $t^* = 1/\acute{\varepsilon}^* = 2.5 \times 10^{-10}$, one hour in the experiments is equivalent to about 450 000

330 years in nature. As our experiments lasted 20 h, this represents around 10 Myr of deformation time
331 in nature at a shortening and extension velocity of 5 $mm.h^{-1}$ in the model and 7.5$mm.yr^{-1}$ in the
332 nature.

333

334 5. Results

335 4.1. M0 experiment: lateral extension with the salt level

336 The M0 model (fig. 6, Movie M0) corresponds to a lateral extension at a 5 $mm.h^{-1}$ rate. This model is
337 composed of 4 layers consisting of 5 mm of barite + pure silicone covered by 1 cm thick and sand, 5
338 mm thick of pure silicone, and 5 mm thick of sand (fig. 5). We sprinkled a thin layer of blue sand on a
339 grid at the top of the first sand layer to better estimate the final deformation in the deepest part of
340 the model.

341 Deep structures are inferred from the top of the lower sand layer (fig. 6A). They consist of four main
342 grabens striking perpendicular to the extension direction and separated by horsts. Horst and graben
343 sizes range between 1 to 5 cm wide and 10 to 60 cm large. In several cases, the lowest layer made of
344 weighted silicone outcrop in the center of the grabens suggesting that the lower sand layer has been
345 thinned (fig. 6A and B). These structures are limited to the right third of the experiment and
346 elsewhere, deep deformations are absent (fig. 6C and D). Deformations related to an extension are
347 also well observed on the right third of the experiment's top surface (fig. 6A). Horsts and grabens
348 strike in the same direction as in-depth and in several grabens, the upper silicon layer also outcrops.
349 At the surface, small grabens are abundant and their sizes are smaller: 0.5 to 3 cm wide and 3 to 30
350 cm large (fig. 6A). Spatial relationships between horsts and grabens located in the lower and the
351 upper sand layers are not straightforward as surface horsts are located over deep grabens and
352 conversely in the case of surface grabens and deep horsts (Fig. 6D). At 5 $mm.h^{-1}$ of extension velocity,
353 the deformation affect the whole experimental area as it starts near the extensional boundary and
354 reach the opposite side of the model at the end of the experiment (fig. 6C, movie M0).

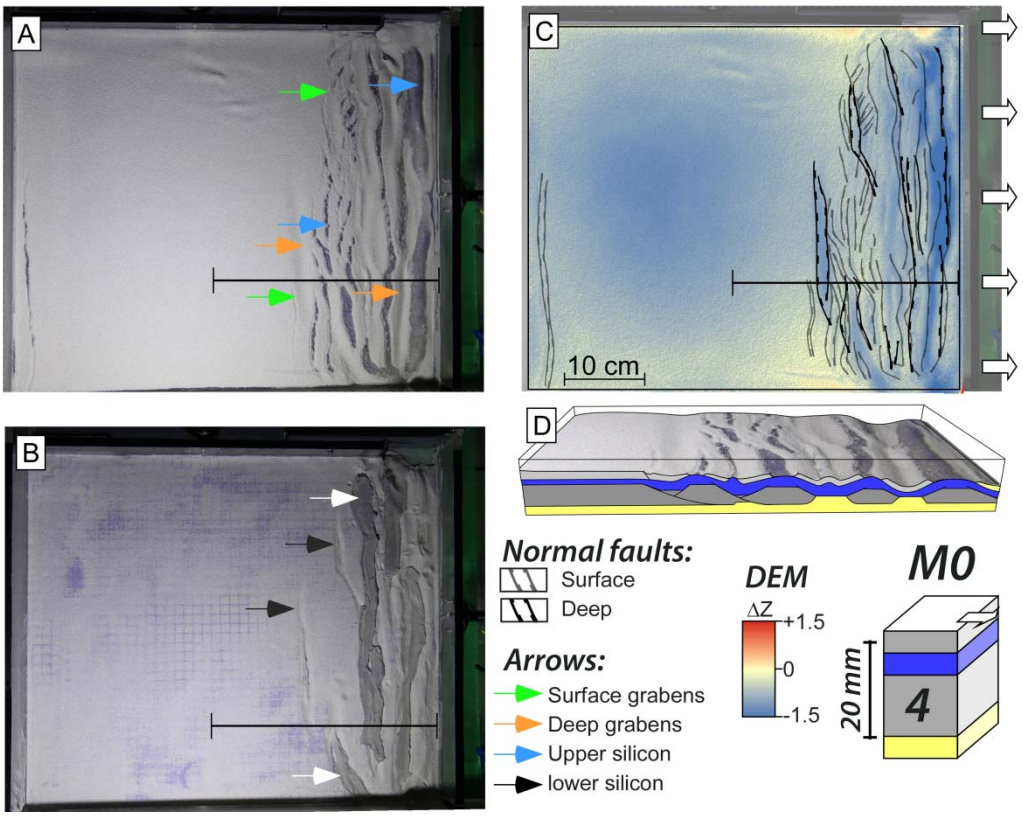

Figure 6: Final stage of the M0 experiment presenting A) the non-interpreted Top Surface picture, B) the Top Lower Sand Layer upper view C) an interpreted map, and D) Perspective view and interpreted cross-section 1: Normal faults crossing the Upper Sand Layer, 2: Normal faults crossing the Lower Sand layer, 3: Pure silicone reaching the model surface, 4: Weighted silicone reaching the Lower Sand layer top. Arrows point several surface and deep structures : Green: upper sand layer graben, blue: pure silicone that reach the model surface, orange: the surface signature of grabens affecting the lower sand layer, black: lower sand layer grabens and white : weighted silicone that reach the lower sand layer surface. A-B represent the position of the cross-section

4.2. M1 experiment: compression applied to a 2 layers model

In the M1 model, we applied, on a two layers model consisting of weighted silicone at the base and sand at the top, a compression without a décollement layer and lateral extension (fig. 5 and 7). The thickness of the lower crust is 5 mm. During the experiment, deformation is materialized at the surface by the formation of four pop-up structures bounded by conjugated thrust faults (fig. 7A and B). Their size and elevation range from 30 to 50 cm and 5 to 10 cm, respectively, and the mean orientation is perpendicular to the compression. In detail, the pop-up structure exhibit a concave accurate shape suggesting that additional friction are existing on the lateral boundaries of the experimental device (Souloumiac et al., 2012). Strike-slip and extensional structures are absent. The first pop-up structure appears near the mobile border and then the deformation progressively propagates into the model (fig. 7A ; movie M1). The last activated pop-up structure is located very close to the opposite experimental device edge suggesting that the décollement layer is activated below most of the device.

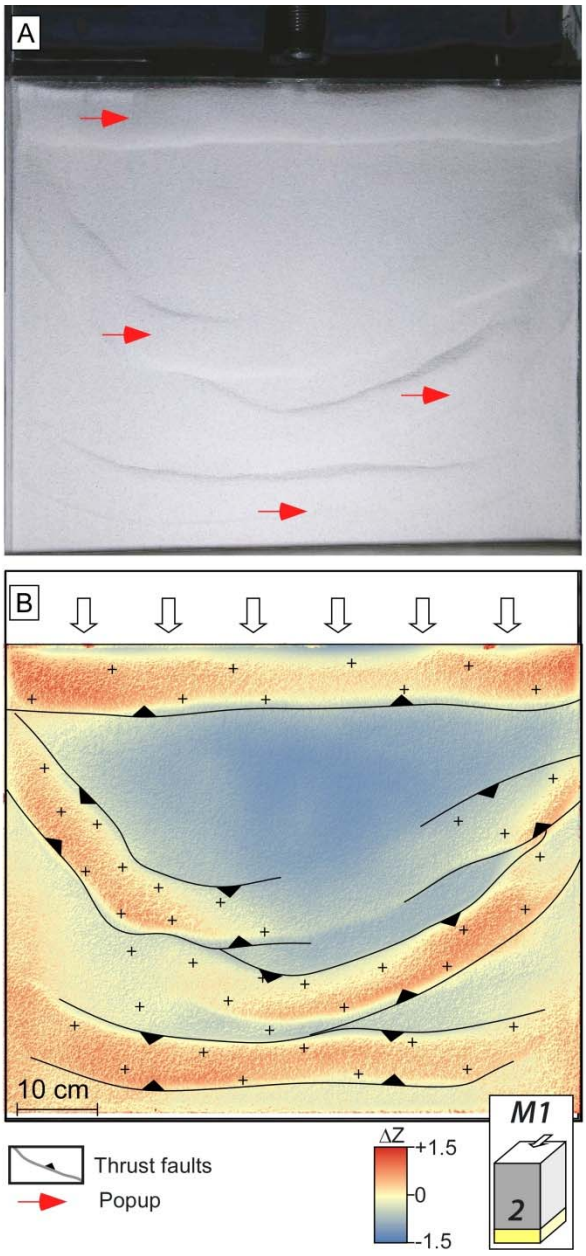

Figure 7: Results of the M1 experiment presenting A) non-interpreted top view of the sand layer and B) the interpreted final stage plotted on top of the surface topography.

4.3. M2 experiment: compression applied to a 4 layers model

The M2 experiment rheology is composed of 4 layers as in the case of M0 but here, shortening rather than extension is applied for 20 hours at a velocity of 5 $mm.h^{-1}$ (fig. 5 and 8).

Deep structures are inferred from the top of the lower sand layer and are located in the half part of the experiment that is bounded by the moving edge (fig. 8B). They consist of two mains pop-up structures striking perpendicular to the shortening direction and located near the moveable edge of the experiment. Pop-up sizes range between 2 to 5 cm wide and 40 to 60 cm large. Besides, a thrust, with a very similar strike and dipping in the direction of the moveable edge is located near the center of the experiment (fig. 8A). Elsewhere on the top of the lower sand layer, deep deformations are absent. M2 experiment's surface deformations occupied a larger area than the deep structures (fig.

8C). Two types of structures are observed: 1) 0.5 to 1 cm wide and 5 to 15 cm large folds, striking mostly perpendicular to the shortening direction, and 2) Normal faults, striking parallel to the large folds exhuming the upper silicon layer up to the model surface. Surface Folds are mostly located in area where uplift is absent, whereas normal faults are observed at the top of the lower sand layer pop-up structures (fig. 8A).

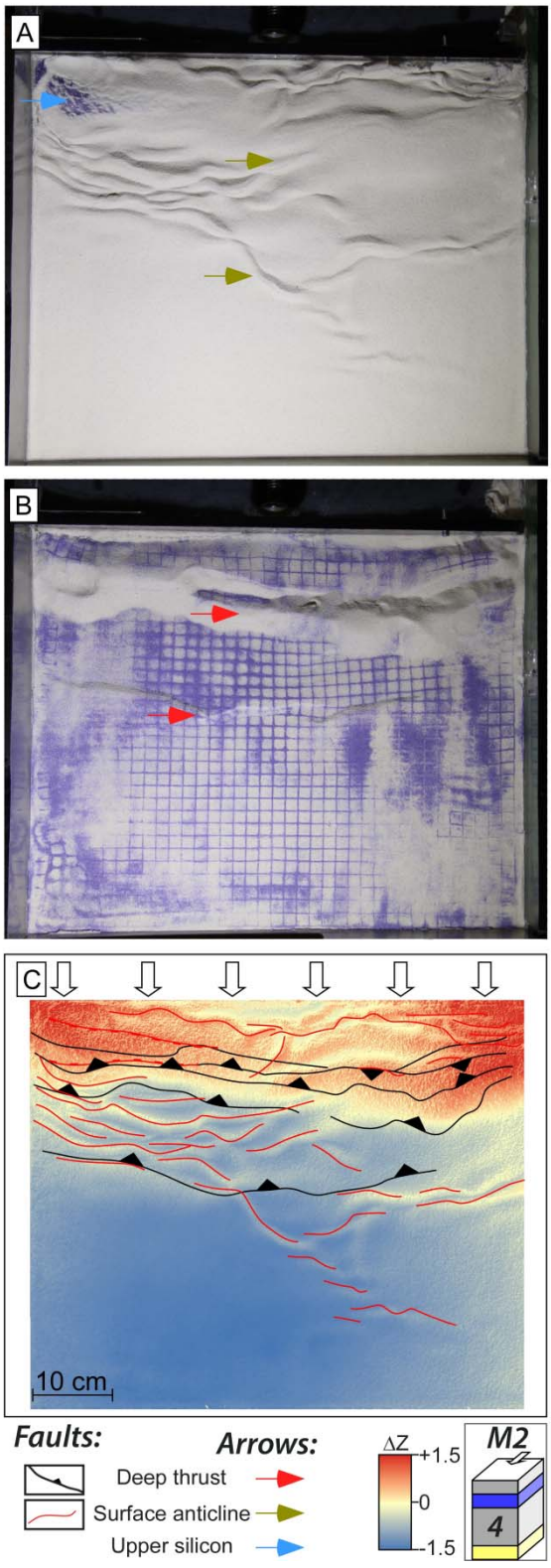

Figure 8: Results of the M2 final stage experiment presenting A) a non-interpreted top view of the upper sand layer and B) a non-interpreted top view of the lower sand layer and C) the structural interpretation plotted on top of the surface topography.

4.4. M3 experiment: compression and lateral extension applied to a 2 layers model

The M3 experiment (fig.9) corresponds to coeval and perpendicular compression and extension applied to the same two layers model rheology used for the M1 experiment (fig. 7). A similar 5 $mm.h^{-1}$ deformation velocity is applied in each direction (fig. 5). Surface deformation consists of two 3 to 5 cm large pop-up structures associated with conjugated strike-slip faults interacting with grabens (fig.9A). As in the case of the M1 experiment, the first pop-up structure appears near the mobile border/backstop (Movie M3). At the same time, a graben starts to extend all along the extensional mobile border/backstop. Then, two conjugated strike-slip faults located on the right part of the experiment start to move suggesting/indicating that both extensions from the right and compression from the top propagate toward the middle of the model (fig.9A). Finally, a second pop-up structure appears near the lower edge of the experiment. It is bounded by two conjugated strike-slip faults: one on the right consists of a transtensive strike-slip fault already active during earlier stage of the experiment and the other is a newly formed transpressive right lateral strike slip fault one located near the left edge of the experiment (fig.9B). As in the case of the M1 experiment, the position of the last activated pop-up structure, very close to the edge of the experimental device, suggests that a décollement layer is activated below most of the device within the silicone layer.

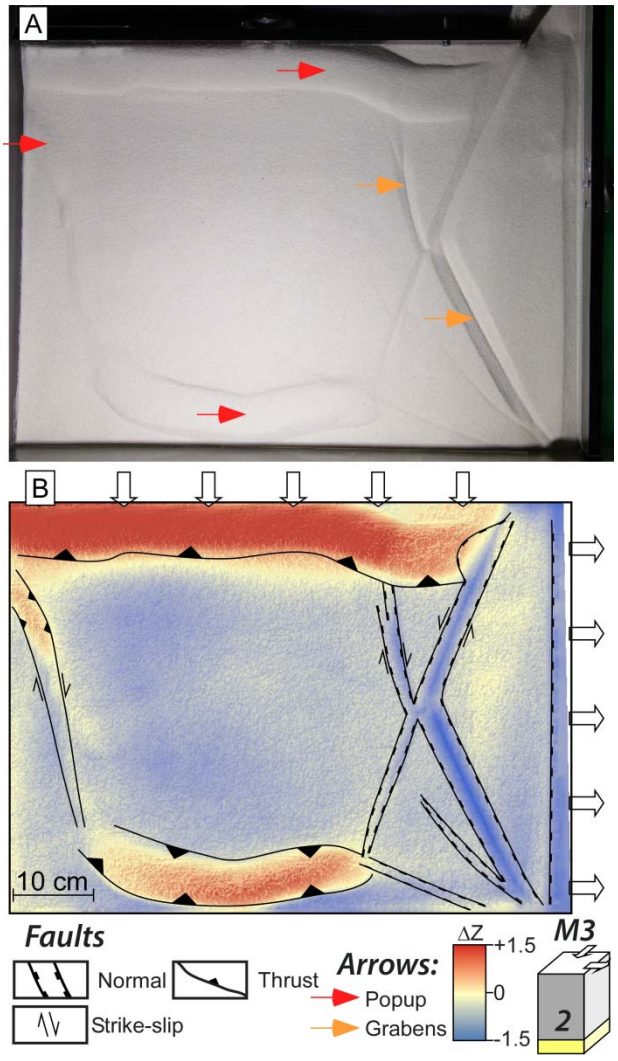

Figure 9: Results of the M3 experiment presenting A) non-interpreted top view of the sand layer and B) the interpreted final stage plotted on top of the surface topography.

4.5. M4 experiment: compression and lateral extension applied to a 4 layers model

In the M4 experiment, we applied coeval and perpendicular compression and extension, as in the case of the M3 experiment, to a 4 layers model sharing the same rheology as the M2 experiment (Fig. 5 and 10). We sprinkled a thin layer of blue sand on a grid at the top of the first sand layer. The final stage is documented with a top view of the experiment surface (fig.10A), a top view of the first sand layer (fig.10C) and, an interpretative final stage sketch (fig.10B). We also show surface top view and instantaneous velocities at the beginning, the middle, and at the end of the experiment (fig.11).

At the final stage, the model topography is characterized by a progressive decrease in altitude from the compressive mobile border/backstop toward the opposite model boundary (fig.10A). The observed surface deformations are mostly compressional and extensional structures (fig.10A and B). About 70 compressive structures are distributed on a large portion of the experiment. They are mostly present on the top half of the experiment where compression is applied and absent on the lower-left corner (Fig 11-Y velocities after 1200 mn). these is 5 to 10 mm thick, 3 to 5 mm high, and 20 to 60 mm large. Due to the small thickness and height, these structures look more like folds than pop-up structures as observed in the M1 and M3 experiments. Besides, several of these compressive structures present an asymmetry suggesting the overturn of the fold axis. The mean fold orientation is orthogonal to the compression direction but an important dispersion of the orientation is locally observed (fig.10B). These later are associated and follow a preferential direction of alignment: parallel or slightly oblique to the compressive mobile border/backstop (fig.10B). X and Y velocities changes across these structures are highlight by PIV imaging (Fig 11-W and Y velocities after 1200 mn) indicate that these echelon fold are related to strike slip tectonics (fig.10A).

Grabens are visible at the surface of the M4 model from two distinct groups (fig.10B). The first one consists of grabens mostly located on the right half of the experiment. Their mean size is 5 to 10 mm thick, 3 to 5 mm high and 20 to 60 mm large and orientations are parallel to the extensive mobile border/backstop. The second group is located near the compressive mobile border/backstop. It consists of a large (30 to 40 mm thick, 400 to 600 mm large) grabens where the upper sand layer is stretched leading the upper silicone layer to reach the model surface (fig.10A). This major structure is associated with several minor (3-5 mm thick 20 to 30 mm large) and perpendicular grabens oriented in the same way as those of the first group.

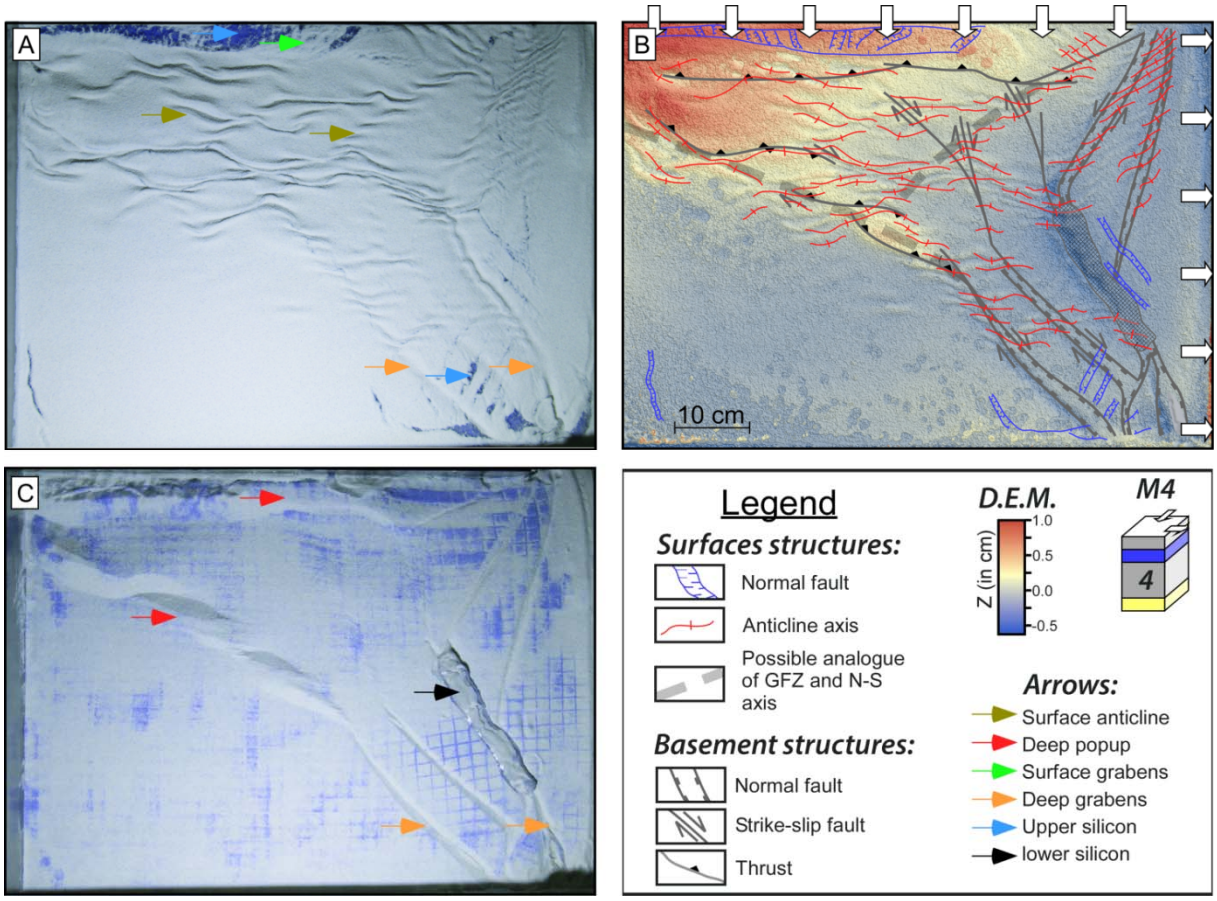

Figure 10: Results of the M4 experiment presenting A) a non-interpreted top view of the upper sand layer and B) a non-interpreted top view of the lower sand layer and C) the interpretation plotted on top surface topography.

In-depth, the top of the first sand layer of the M4 experiment (fig.10C) is characterized by a complex association of pop-up structures, strike-slip faults, and grabens. Four Pop-up structures are located near the compressive moveable border and in the top-left quarter of the experiment. They consist of 30 to 50 mm thick, 5 to 10 mm high structures. The one that is located all along the moveable border is the larger whereas the three others form a 100mm large "en echelon" compressible structure lightly oblique to the compression direction (fig.10B). Graben structures take place near the extensive moveable border and mostly in the base-right part of the experiment. At the exception of a structure located just left from the moveable border, the orientation of graben is oblique to the extension direction suggesting that strike-slip motion is associated with their formations (fig.10B). In the central part of the right side of the model, stretching of the first sand layer reach its maximum with an almost complete thinning (fig.10B). Strike-slip faults are mostly located in the center part of the experiment and evolve from transpressive near the top to transtensive structures near the right edge of the experimental device (fig.10B). At the surface of the model, these deep structures form large and smooth, positive and negative reliefs that are associated or not with smaller-scale structures (fig.10A and B).

Comparisons between surface structures with deformations at the top of the first sand layer (fig.10B) highlight a wide variety of relationships between deep and surface structures. Half of the surface folds are not associated with faults in-depth suggesting a mechanical decoupling between the two

sand layers analog with thin skin tectonics models in nature (fig.10B). The other surface folds are connected with structures in-depth: thrust faults forming the boundary of pop-up structures in the case of folds aligned parallel to the compressive moveable border and strike-slip faults in the case of folds aligned obliquely to the experiment boundaries (fig.10B). In a very similar way, surface grabens located on the top of the experiment are not associated with extension in-depth (fig.10B). This highlights the decoupling role of the upper silicon layer during extension as already evidenced by Belguith et al., 2013.

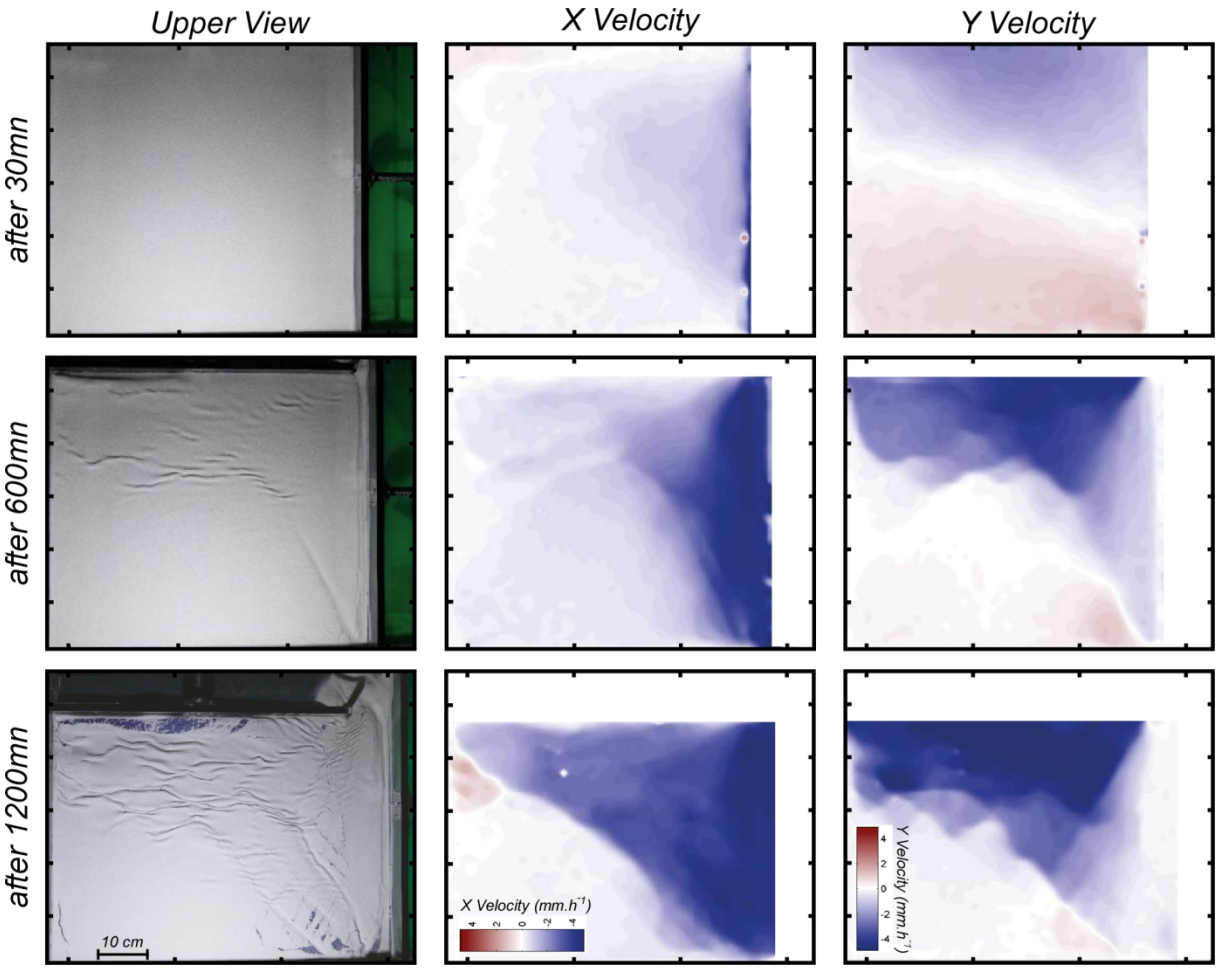

Figure 11: a evolution of the M4 experiment after 30 (2.5%), 600 (50%) and 1200mn(100%) of shortening. Left: upper view picture of the experiment. Center and right: results from particle image velocity analyses in lines (center) and columns.

5. Discussion

"Shortening only" M1 and M2 experiments (fig. 7 and 8) lead to the formation of a tectonics wedge. Compressive structures consist of tens of kilometers wide pop-ups affecting the basement and kilometer scales anticline developing in the upper sedimentary cover (M2 experiment; Fig. 8). In the experiment, grabens are absent and the strike-slip structures are limited to the edge perpendicular to the compressive one. When considering an additional extension orthogonal to the shortening direction (M3 and M4 experiments; Fig. 9 and 10), hosts and grabens, strike-slip pop-ups structures are associated. Grabens are located near the right edge of the experiment and are always transtensive. a dextral strike-slip fault is observed near the left edge of the experimental device.

In a previously proposed experiment with lateral changes of the upper crust thickness (Sokoutis et al., 2001), a very realistic association of strike-slip and thrust faults has been obtained matching well with the tectonic scheme of the Tunisian Atlas. however, no structures compatible with extension are observed on the side of the experimental device corresponding to the Pelagian domain. Assuming an initial stage with constant modeled units thicknesses (Fig. 5), experiment M3 and M4, that consider both shortening and lateral extension, represent the closest simulations of the tectonic pattern of the Tunisian-Pelagian domain (Fig 10).

As a whole, the compressive deformation of the NAAC has been driven by Nubia and Eurasia plates convergence. During the first stage, deformations were localized at the front of the subducting Tethyan slab leading to the burial of material below the internal part of the belt and the stacking of Numidian and Tellian tectonic slice (Fig. 1A). After a slab break-off event initiated at 17 Ma along the Algerian margin and propagating toward the East and the West (Fig. 1D; Maury et al., 2000), the strain is no longer triggered by the Tethyan slab and deformation becomes more diffuse in the NAAC. Despite the absence of still attached subducting slab, several models based on orogenic wedge have been proposed (Frizon de Lamotte et al., 2011, Khomzi et al., 2016) where crustal north dipping thrusts rooted at the brittle-ductile transition of the Africa plate crust. Presented experiment with the mobile edge in compression supports compressive strain localization to the north of the studied area.

Orthogonal extension direction, corresponding in nature to a NE-SW strike, is already proposed in the Pelagiane domain (Fig. 2A). It affects the whole lithosphere (Civile et al., 2010) and is active since the Tortonian as evidenced by the NE Motion of Sicilia relative to Africa (Fig. 3; Serpelloni et al., 2007, Bahrouni et al., 2020). Such a motion and extension are related to the far-field pull of the Western-Hellenic/Dinaride subduction (Belguith et al., 2013).

Considering this, we focus in the following discussion on the possible crustal rooting of the main tectonic structures, the tectonic role of the Triassic evaporite décollement layer, and the relationship between our results and lithospheric scale processes.

5.1. A crustal roots for the main tectonic structures

Within experiment M3 (Fig. 9) and M4 (Fig. 10 and 11), orthogonal to shortening extension lead to the formation of oblique strike-slip structures located on each side of the experiment and rooting into the lower sand layer. Along these, there is a competition between transpressive and transtensive strains as extension and shortening propagate through the experiment (Fig. 11).

- *Sicilian Channel grabens*

On the right side of the experiment, transtensive strain widely dominate and strike-slip structures are associated with horsts and grabens (Fig 9A and 10B). A very similar kind of crustal extension is observed on the Sicilian Channel where strike-slip tectonic is also observed (Fig. 2A and 3). Furthermore, there is a very similar change of extensional structure strike from north to the south both in nature and the experiment (dot 8 on Fig. 12).

- *Thrust faults*

In the lower sand layer, compressive pop-up structures are located near the compressive mobile border and in the top-left quarter of the experiment (fig.10C). These deep structures are responsible for most of the wedge relief as, in the cover, extension affects the upper sand layer when uplifted (fig.10B). The orientation of the thrust faults forming the boundaries of the pop-up structure is in good agreement with the orientation of deep structures such as the Zaghouan thrust fault (dot 6 on Fig. 12: Turki 1985, Morgan et al 1998, Khomsi et al., 2009). Toward the west, the structures leading to the thickening of the continental crust up to 40 km are poorly constrained (fig. 2C). This concerns the relief bounding the Hodna basin to the NE in Algeria and the Aures mountains (dot 2 on Fig. 12; Rabaute and Chamot-Rooke, 2014). Results from the M4 experiment suggest here the occurrence of an "en échelon" pop-up structure leading to the thickening of the crust and the formation of the highest relief here (fig.10B).

Geological Cross-sections of the Central Atlas have proposed the possible occurrence of thrust faults affecting the basement associated with a décollement layer located at the base of the Mesozoic cover (Khomsi et al., 2016, 2019, Leprêtre et al., 2018). Our experimental results tend to confirm this hypothese with a lower number and a bigger size of crustal pop-up block (fig.10C). As the pop-up size is constrained in the experiment by the lower sand layer thickness, we propose, in agreement with Khomsi et al., 2016, Leprêtre et al., 2018, that inherited normal faults dated from Mesozoic time (Soussi, 2002; Boughdiri et al., 2007) may have been bounded smaller inverted blocks.

- *the Gafsa Fault zone*

To the left side of the experiment M3 (Fig. 9B) and M4 (Fig. 10B), dextral strike-slip fault forms the boundary between deformed (to the upper-right) and undeformed (to the lower-left corner) parts of the experiment. Undeformed area, that is immobile during the whole experiment (Fig. 11) because of friction on the left and bottom walls (Souloumiac et al., 2012), corresponds to the Saharian plateform whereas the deformed area correspond to the Atlas and Pelagian domains.

This dextral strike-slip fault evolves from transpressive (pop-ups) to transtensive (grabens) strain (Fig. 10). In nature, the Gafsa Fault zone characterized at the surface by strong changes on the Djebels orientations (fig. 2), seismic activities (Fig. 3: Bahrouni et al., 2014, Soumaya et al., 2015), and changes of the geodetic motions (Fig. 3: Bougrine et al., 2019, Bahrouni et al., 2020). The intensity of compressive tectonic decreases all along the Gafsa Fault zone from the NW to the SE. North to the "Chott el Jerid" area, tectonic (Saïd et al., 2011, Bahrouni et al., 2014), geodetic (Bougrine et al., 2019, Bahrouni et al., 2020), and seismological (Vannucci et al., 2004, Soumaya et al., 2015) evidence lead to conclude on a transpressive strain of this contact (Fig. 3). Data are scarcer south to the "Chott el jerid" (fig. 2), however seismological results suggest that the strike-slip tectonic regime becomes very similar to those of the Pelagian Domain with the domination of NE-SW direction of extension (Soumaya et al., 2015). We propose that the large dextral transpressive to transtensive strike-slip zone located on the left side of M4 represents an analog of the Gafsa fault zone (dot 4 on Fig. 12). In the M4 experiment, the deep crustal pop-up structure observed along the transpressive part of the fault may correspond to the high relief of the Aures Mountain that may be uplifted in this case by thrusts rooting in the basement (dot 4 on Fig. 12). Such a possibility has already been proposed based on seismological and geodetic data (Bahrouni et al., 2020).

- *the N-S axis*

On the M4 wedge (Fig.10), the transition between transtensive to transpressive strike-slip tectonics in the deeper sand layer occurred on the right half of the experiment where several dextral strike-slip faults associated with minor displacements are not affected by the extension. No equivalent of these deep structures has been described in nature (Fig. 2 and 3). On the surface, several "en echelon" folds are located between the main deep thrust and the left-lateral strike-slip fault (dot 5 on Fig. 12). These are compatible with a sinistral and transpressive strike-slip motion that may affect the upper sand layer only. In nature (Fig. 2 and 3), the N-S axis stands in a very similar position and is also affected by the same motion (Rigane and Gourmelen, 2011). As in the experiment, it is also bounded to the north by deeply rooted thrust structures as evidenced by seismic activity (Soumaya et al., 2015). On seismic line crossing the N-S axis (Khomsi et al., 2009), the relationships between structures observed in the cover and the basement are not straightforward as also observed in experiment M4 (Fig. 10 A and C).

As a whole, we propose that extension orthogonal to shortening when especially applied to a 4 layers model can reproduce in the laboratory the main strike-slip boundary such as Gafsa fault zone and N-S axis and crustal-scale rift as observed in the Sicily channel (Fig. 12).

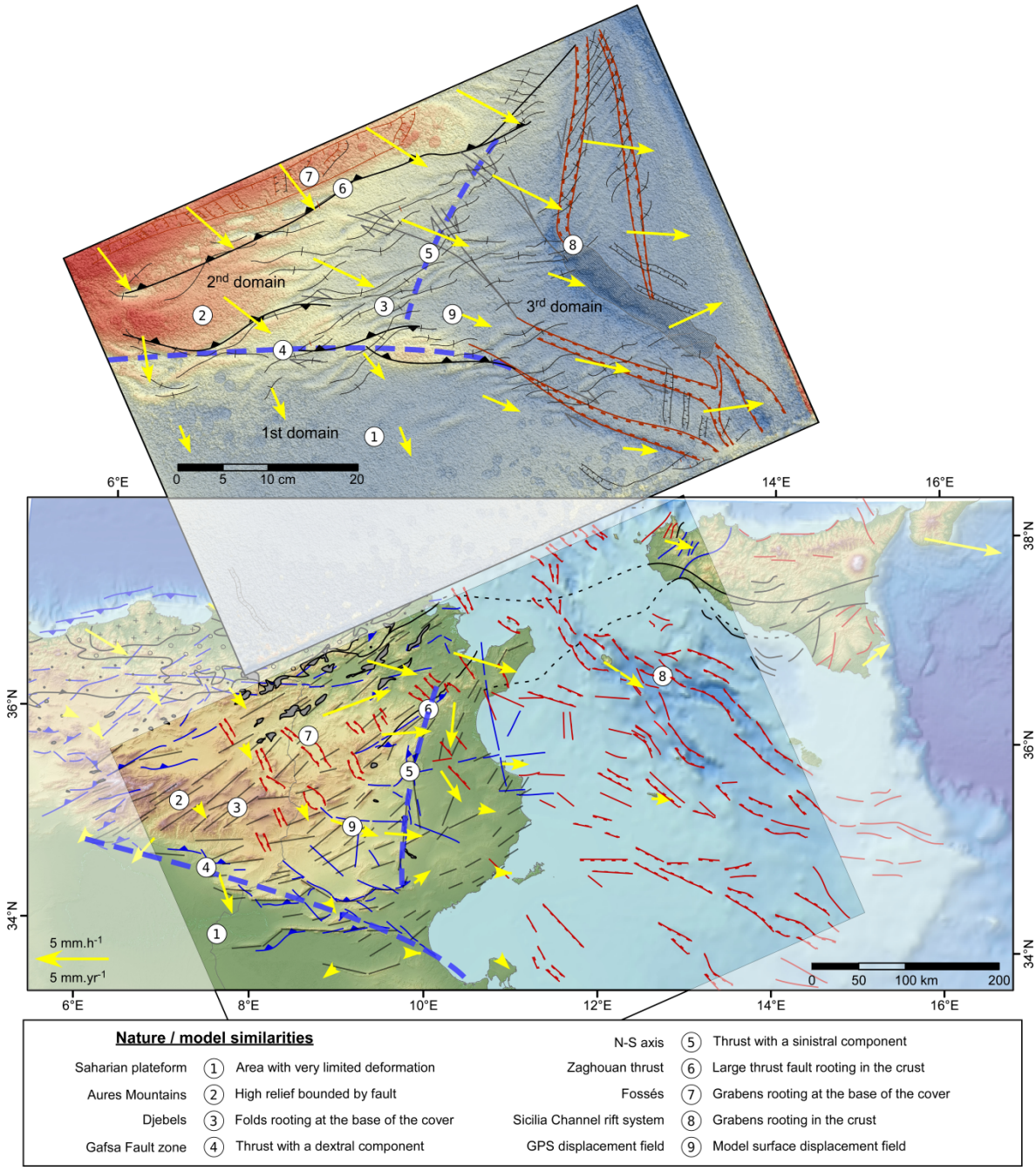

Figure 12. Comparison of the tectonic and morphological features between the final stage of the M4 experiment (top, see Fig. 10 for the legend) and the eastern termination of the NAAC (bottom, see fig. 2A for the legend). Nature / model similarities are labeled from west to east. Dashed thick blue line represent the Gafsa fault zone (to the SW) and the N-S axis (to the E). Yellow arrows represent, the GPS data plotted assuming a fixed Saharian plateform in the natural case and the velocity surface field deduce from PIV imaging (Fig. 11) and assuming a fixed area located at the bottom-left corner of the experiment M4. Maps and displacement field of nature and model are displayed at a scale respecting experimental ratio of 1.2E-06 for the length and 5.26E+03 for the speed (Table 1).

5.2. An Atlassic triassic evaporite décollement layer

By taking into account the second silicone and sand layers, M2 and M4 experiments (Fig. 5) investigated the role of a possible evaporitic décollement layer located at the base of the Atlassic Mesozoic cover.

- *"décollement layer"*

At the surface, numerous compressive structures, formed during the M2 (Fig.8) and M4 experiments (fig.10), appear similar in size and number to the djebels in the Central Atlas (dot 3 on fig. 12). Observations at the top of the lower sand layer suggest that most of these structures, located between the main crustal thrust and the equivalent of the Gafsa fault zone, root into the upper silicone layer and do not affect the lower sand layer. This observation is in good agreement with thin-skinned models that are proposed for the formation of Atlassic NE-SW directed Djebels (Morgan et al 1998, Khomsi et al., 2009, 2016, Aridhi et al 2013).

In the M4 experiment, the extension is not restricted to crustal-scale processes located on the right side of the model (dot 8 on Fig. 12), it affects also the uplifted part where it starts as the tectonic wedge is already well developed (fig.10B). Such a similar relationship is inferred from structural studies on the "fossé area" where extension postdates the local shortening (Fig. 2A; Belguith et al., 2011). Here, results taken from the M4 experiment suggests that the extension does not affect the lower sand layer (Fig. 10C). In the northern Atlas, similar results are obtained by Belguith et al. (2013) who propose that the horsts and the grabens root at the base of the Mesozoic cover. In experiment M4 and nature, the position of these grabens at the top of the sand wedge suggests that the extension has to deal with gravity processes and relief together with a regional orthogonal extension (dot 7 on fig.12).

- *Impact on wedge dynamic and tectonics inversion*

The occurrence of a décollement layer at the base of the sedimentary cover is not only responsible for thin skin tectonics, but it also affects the wedge dynamics as a whole: in absence of such a layer (M1 and M3 experiments), crustal orogenic wedge reaches the boundary of the experimental device (Fig. 7 and 9) whereas it is restricted to the two thirds when a décollement layer is introduced (Fig. 8 and 10). As also observed on tectonic wedges affected by erosion (Henriquet et al., 2020), extension at the wedge top reduces the surface slope and maintain under-critical internal stress. The resulting deformations are underplating that increases the surface slope and limits the frontal propagation of the crustal deformation. In such a context of underplating, the frontal part of the wedge present a very different aspect as a large oblique strike-slip structure on the left side and several grabens on the right side of the experiment device mimic the Gafsa fault zone and the Sicilian channel grabens (dot 8 on Fig. 12).

In the right side of the M4 experiment (Fig. 10), and as in the Sicilian channel (Fig. 2), timing is different since shortening post-date the extensional phase (Civile et al., 2008, Ben Brahim et al., 2013, Cavallaro et al., 2017). We inferred from experimental results that during the first half of the M4 experiment, the extension is spreading quickly to the right corner of the device whereas the tectonic wedge is restricted to the top (fig.10). During the second half of the experiment, the growing wedge is spreading to the base of the experiment and early grabens located in the third domain are inverted. Thus we propose that opposite timings between extension and tectonics in the Atlas domain and the Pelagian sea are the consequence of southward growth of the tectonic wedge and the westward propagation of extension since the Tortonian.

5.3. Limits of the model and relationship with lithospheric scale processes

In both nature (Fig. 2; Belguith et al., 2011, Bahrouni et al., 2014) and experiment (fig.10) the extension observed in the Atlas domain presents a multidirectional component as two orthogonal directions (NE-SW and NW-SE) coexists (dot 7 on fig 12). In Northern Atlas, the major NE–SW extension locally predates the NW–SE-trending extension and these two directions of extension postdate the shortening phase (Belguith et al., 2011). In the experiment M4, two orthogonal directions coexist in the equivalent of the Northern Atlas domain; here, the extension in the same direction than shortening is the most visible (Fig. 10A). As we proposed that gravity processes play a key role in the formation of extension affecting the upper sand layer at the top of the wedge, such a difference between model and nature can be explained by a difference in slopes: a) extension in the same direction than shortening is enhanced by South-East verging basement-cover wedge slope and b) extension orthogonal to shortening direction is triggered by North-East verging slope from the Atlas mountains toward the Pelagian sea (Fig 2A and 12).

Considering the limited thickness and the absence lower crust and mantle analogs, the modeled wedge is unable to produce a crustal root as awaited in nature and observed below the NAAC (Fig. 2C). This results in an overestimation of model relief and wedge slope (Fig. 10B) enhancing extension in the direction of shortening. Furthermore, it has been proposed that the Africa plate lithosphere is delaminating below the NAAC (Fig 1B; Roure et al., 2012, Booth-Rea et al., 2018). The delaminating slab is bounded to the south by a STEP fault that follows at the surface the Gafsa fault zone and is connected to the African lithosphere below the North-South Axis (Fig 1B; Booth-Rea et al., 2018). Uplift of the Atlassic domain associated with subsidence in the Pelagian sea is a possible direct consequence of slab delamination that is potentially responsible for drainage reworking in the Northern Tunisian (Camafort et al., 2020).

Considering these, we propose that uplift and subsidence in the Atlas and Pelagian areas are the consequence of lithospheric delamination and the formation of a crustal root below Atlassic wedge, respectively. These could have changed analog surface wedge slope and have possibly enhanced the NE-SW direction of extension at the top of the Atlassic wedge (Fig. 1B).

6. Conclusion

Analog modeling of shortening and orthogonal extension directions applied to a 4 layers model have provided noteworthy/remarquable similarities with the Tortonian-to-present geological/geodynamic evolution of eastern Algeria, Tunisian and Pelagian sea regarding the relief formation, the structural pattern, and the present-day surface motion (Fig. 12).

1) Coexisting horts and grabens, thrusts, and strike-slip faults are produced when the analog model is affected both by shortening and orthogonal extension directions. This confirms the regional setting where shortening is related to convergence between Nubia and Eurasia plates. According to Belguith et al., (2013), we propose that crustal extension is related/driven by to the far-field pull of the Western-Hellenic/Dinaride subduction.

2) Several tectonics structures affect the basement and lead to the formation of crustal-scale thrusts and grabens striking parallel to the model edges. These correspond to (a) basement thrusts located below the tectonic wedge are similar to a structure like the Zaghouan thrust faults (Morgan et al., 1998, Khomsi et al., 2009), (b) crustal-scale grabens that resemble the Sicilian Channel grabens (Civile

et al., 2010) and (c) deep sinistral strike-slip structures that particularly match with the Gafsa Fault zone.

3) 4 layers model experiment submitted to compression and lateral extension lead to the formation of a décollement layer at the base of the sedimentary cover where several structures related to shortening and extension roots. Their position, strike, and size are analogue to first, the Eastern Algerian and Tunisian "djebels" in the case of folds and second, to the "fossés" located in the northern Atlas in the case of the grabens. Thus the Atlas Triassic evaporite rocks act as a décollement layer both for compressive and extensive structures.

4) Extension at the top of the tectonic wedge reduces its surface slope and favors underthrusting in the basement. Such a process may explain the compressive strain localization in the basement along the Zaghouan thrust, leading to the formation of strike-slip faults associated with orthogonal crustal extension in the frontal part of the wedge, as observed in the Gafsa fault zone and in the Silician channel rift system.

5) Misfit on mostly expressed extension direction at the wedge top between model and nature highlights the role of lithospheric scale processes in the possible eastward tilting of Atlasic wedge: the opposite vertical motions between Atlas and Pelagian areas as a consequence of lithospheric delamination could have tilted the surface wedge slope toward the NE and have possibly enhanced the NE-SW direction of extension in the "fossé" area.

Acknowledgments:

Stéphane Dominguez is greatly acknowledged fir his comments on experiments and early version of the article. We are grateful to the Editor Philippe Agard, to Bertrand Maillot and to another reviewers for their constructive comments.

References

Adam, J., Urai, J. L., Wieneke, B., Oncken, O., Pfeiffer, K., Kukowski, N., et al. (2005). Shear localisation and strain distribution during tectonic faulting - New insights from granular-flow experiments and high-resolution optical image correlation techniques. *Journal of Structural Geology*. https://doi.org/10.1016/j.jsg.2004.08.008

Ahmadi, R., Mercier, E., & Ouali, J. (2013). Growth-strata geometry in fault-propagation folds: A case study from the Gafsa basin, southern Tunisian Atlas. *Swiss Journal of Geosciences*. https://doi.org/10.1007/s00015-013-0122-z

Aïte, M.O., Gélard, J.P., (1997). Distension néogène post-collisionnelle sur le transect de Grande-Kabylie (Algérie). Bull. la Soc. Geol. Fr. 168, 423–436.

Altamimi, Z., Métivier, L., Rebischung, P., Rouby, H., & Collilieux, X. (2017). ITRF2014 plate motion model. *Geophysical Journal International*. https://doi.org/10.1093/gji/ggx136

Arab, M., Maherssi, C. EL, Granjeon, D., Roure, F., Déverchère, J., Cuilhé, L., Hassaim, M., Mouchot, N., Doublet, S., Khomsi, S., (2020). On the origin and consequences of crustal-scale extension between Africa and Sicily since Late Miocene: insights from the Kaboudia area, western Pelagian Sea. Tectonophysics. https://doi.org/10.1016/j.tecto.2020.228565

Argnani, A. (1990). The strait of sicily rift zone: Foreland deformation related to the evolution of a

back-arc basin. *Journal of Geodynamics*. https://doi.org/10.1016/0264-3707(90)90028-S

Argus, D. F., Gordon, R. G., & Demets, C. (2011). Geologically current motion of 56 plates relative to the no-net-rotation reference frame. *Geochemistry, Geophysics, Geosystems*. https://doi.org/10.1029/2011GC003751

Aridhi, K., Aridhi, S., Bagga, M. A. O., Abdeljaouad, S., Zargouni, F., & Mercier, E. (2013). Paleogeographical restoration and ramp tectonic evidence in Tunisian Tellian domain: Ain El Bey-Bou Awen area. *Arabian Journal of Geosciences*. https://doi.org/10.1007/s12517-011-0447-8

Bahrouni, N., Bouaziz, S., Soumaya, A., Ben Ayed, N., Attafi, K., Houla, Y., et al. (2014). Neotectonic and seismotectonic investigation of seismically active regions in Tunisia: A multidisciplinary approach. *Journal of Seismology*. https://doi.org/10.1007/s10950-013-9395-y

Bahrouni, N., Masson, F., Meghraoui, M., Saleh, M., Maamri, R., Dhaha, F., Arfaoui, M., (2020). Active tectonics and GPS data analysis of the Maghrebian thrust belt and Africa-Eurasia plate convergence in Tunisia. Tectonophysics. https://doi.org/10.1016/j.tecto.2020.228440

Belguith, Y., Geoffroy, L., Rigane, A., Gourmelen, C., & Dhia, H. Ben. (2011). Neogene extensional deformation and related stress regimes in central Tunisia. *Tectonophysics*. https://doi.org/10.1016/j.tecto.2011.06.009

Belguith, Y., Geoffroy, L., Mourgues, R., & Rigane, A. (2013). Analogue modelling of Late Miocene-Early Quaternary continental crustal extension in the Tunisia-Sicily Channel area. *Tectonophysics*. https://doi.org/10.1016/j.tecto.2013.08.023

Booth-Rea, G., Gaidi, S., Melki, F., Marzougui, W., Azañón, J.M., Zargouni, F., Galvé, J.P., Pérez-Peña, J. V., 2018. Late Miocene Extensional Collapse of Northern Tunisia. Tectonics. https://doi.org/10.1029/2017TC004846

Boschi, L., Faccenna, C., & Becker, T. W. (2010). Mantle structure and dynamic topography in the Mediterranean Basin. *Geophysical Research Letters*. https://doi.org/10.1029/2010GL045001

Bouaziz, S., Barrier, E., Soussi, M., Turki, M. M., & Zouari, H. (2002). Tectonic evolution of the northern African margin in Tunisia from paleostress data and sedimentary record. *Tectonophysics*. https://doi.org/10.1016/S0040-1951(02)00370-0

Boudiaf, A., Philip, H., Coutelle, A., & Ritz, J. F. (1999). Evidence of a major quaternary thrust fault in southern Kabylie (Algeria). *Geodinamica Acta*. https://doi.org/10.1016/S0985-3111(99)80024-2

Boughdiri, M., Cordey, F., Sallouhi, H., Maâlaoui, K., Masrouhi, A., & Soussi, M. (2007). Jurassic radiolarian-bearing series of Tunisia: Biostratigraphy and significance to western tethys correlations. *Swiss Journal of Geosciences*. https://doi.org/10.1007/s00015-007-1237-x

Bougrine, A., Yelles-Chaouche, A. K., & Calais, E. (2019). Active deformation in Algeria from continuous GPS measurements. *Geophysical Journal International*. https://doi.org/10.1093/gji/ggz035

Brahim, G. Ben, Brahim, N., & Turki, F. (2013). Neogene tectonic evolution of the Gulf of Hammamet area, Northeast Tunisia offshore. *Journal of African Earth Sciences*. https://doi.org/10.1016/j.jafrearsci.2013.01.009

Ben Brahim, G., Ahmadi, R., Brahim, N., & Turki, F. (2014). Neogene tectonics and fault-related folds in the Gulf of Hammamet area, Tunisian offshore. *Journal of African Earth Sciences*.

https://doi.org/10.1016/j.jafrearsci.2014.04.029

Burollet, P.F., 1956. Contribution à l'étude stratigraphique de la Tunisie centrale. Ann. Mines Géol. Tunis, vol. 18, 350p.

Caire, A., 1977. Interprétation tectonique unitaire de l'Atlas tunisien à fossés. C. R. Acad. Sci. Paris D, 284, 349–352.

Calais, E., DeMets, C., & Nocquet, J. M. (2003). Evidence for a post-3.16-Ma change in Nubia-Eurasia-North America plate motions? *Earth and Planetary Science Letters*. https://doi.org/10.1016/S0012-821X(03)00482-5

Camafort, M., Pérez-Peña, J. V., Booth-Rea, G., Melki, F., Gràcia, E., Azañón, J.M., Galve, J.P., Marzougui, W., Gaidi, S., Ranero, C.R., 2020. Active tectonics and drainage evolution in the Tunisian Atlas driven by interaction between crustal shortening and mantle dynamics. Geomorphology. https://doi.org/10.1016/j.geomorph.2019.106954

Carminati, E., Wortel, M. J. R., Meijer, P. T., & Sabadini, R. (1998). The two-stage opening of the western-central Mediterranean basins: A forward modeling test to a new evolutionary model. *Earth and Planetary Science Letters*. https://doi.org/10.1016/S0012-821X(98)00119-8

Catalano, R., Di Stefano, P., & Vitale, F. P. (1995). Structural trends and palaeogeography of the central and western Sicily belt: new insights. *Terra Nova*. https://doi.org/10.1111/j.1365-3121.1995.tb00688.x

Cavallaro, D., Monaco, C., Polonia, A., Sulli, A., & Di Stefano, A. (2017). Evidence of positive tectonic inversion in the north-central sector of the Sicily Channel (Central Mediterranean). *Natural Hazards*. https://doi.org/10.1007/s11069-016-2515-6

Chertova, M. V., Spakman, W., Geenen, T., Van Den Berg, A. P., & Van Hinsbergen, D. J. J. (2014). Underpinning tectonic reconstructions of the western Mediterranean region with dynamic slab evolution from 3-D numerical modeling. *Journal of Geophysical Research: Solid Earth*. https://doi.org/10.1002/2014JB011150

Chihi, L., Philip, H. (1998). Les fossés de l'extrémité orientale du Maghreb (Tunisie et Algérie 502 orientale) : tectonique mio-plio-quaternaire et implication dans l'évolution 20 503 géodynamique récente de la Méditerranée occidentale. *Notes Service Géologique.* 504 Tunisie, 64, 103-116.

Civile, D., Lodolo, E., Tortorici, L., Lanzafame, G., & Brancolini, G. (2008). Relationships between magmatism and tectonics in a continental rift: The Pantelleria Island region (Sicily Channel, Italy). *Marine Geology*. https://doi.org/10.1016/j.margeo.2008.01.009

Civile, D., Lodolo, E., Accettella, D., Geletti, R., Ben-Avraham, Z., Deponte, M., et al. (2010). The Pantelleria graben (Sicily Channel, Central Mediterranean): An example of intraplate "passive" rift. *Tectonophysics*. https://doi.org/10.1016/j.tecto.2010.05.008

Corti, G., Lucia, S., Bonini, M., Sani, F., & Mazzarini, F. (2006). Interaction between normal faults and pre-existing thrust systems in analogue models. *Geological Society Special Publication*. https://doi.org/10.1144/GSL.SP.2006.253.01.03

Davy, Ph, & Cobbold, P. R. (1991). Experiments on shortening of a 4-layer model of the continental lithosphere. *Tectonophysics*. https://doi.org/10.1016/0040-1951(91)90311-F

Davy, Philippe, & Cobbold, P. R. (1988). Indentation tectonics in nature and experiment. 1.

Experiments scaled for gravity. *Bull. Geol. Inst. Univ. Uppsala, NS*.

DeMets, C., Iaffaldano, G., & Merkouriev, S. (2015). High-resolution Neogene and Quaternary estimates of Nubia-Eurasia-North America Plate motion. *Geophysical Journal International*. https://doi.org/10.1093/gji/ggv277

Déverchère, J., Yelles, K., Domzig, A., Mercier de Lépinay, B., Bouillin, J. P., Gaullier, V., et al. (2005). Active thrust faulting offshore offshore Boumerdes, Algeria, and its relations to the 2003 Mw 6.9 earthquake. *Geophysical Research Letters*. https://doi.org/10.1029/2004GL021646

Dewey, J. F., Helman, M. L., Knott, S. D., Turco, E., & Hutton, D. H. W. (1989). Kinematics of the western Mediterranean. *Geological Society Special Publication*. https://doi.org/10.1144/GSL.SP.1989.045.01.15

Domzig, A., Yelles, K., Le Roy, C., Déverchère, J., Bouillin, J. P., Bracène, R., et al. (2006). Searching for the Africa-Eurasia Miocene boundary offshore western Algeria (MARADJA'03 cruise). *Comptes Rendus - Geoscience*. https://doi.org/10.1016/j.crte.2005.11.009

Faccenna, C., Piromallo, C., Crespo-Blanc, A., Jolivet, L., & Rossetti, F. (2004). Lateral slab deformation and the origin of the western Mediterranean arcs. *Tectonics*. https://doi.org/10.1029/2002TC001488

Fedorik, J., Toscani, G., Lodolo, E., Civile, D., Bonini, L., & Seno, S. (2018). Structural analysis and Miocene-to-Present tectonic evolution of a lithospheric-scale, transcurrent lineament: The Sciacca Fault (Sicilian Channel, Central Mediterranean Sea). *Tectonophysics*. https://doi.org/10.1016/j.tecto.2017.11.014

Fichtner, A., & Villaseñor, A. (2015). Crust and upper mantle of the western Mediterranean - Constraints from full-waveform inversion. *Earth and Planetary Science Letters*. https://doi.org/10.1016/j.epsl.2015.07.038

Gharbi, M., Masrouhi, A., Espurt, N., Bellier, O., Amari, E. A., Ben Youssef, M., & Ghanmi, M. (2013). New tectono-sedimentary evidences for Aptian to Santonian extension of the Cretaceous rifting in the northern Chotts range (southern Tunisia). *Journal of African Earth Sciences*. https://doi.org/10.1016/j.jafrearsci.2012.09.017

Globig, J., Fernàndez, M., Torne, M., Vergés, J., Robert, A., Faccenna, C., 2016. New insights into the crust and lithospheric mantle structure of Africa from elevation, geoid, and thermal analysis. J. Geophys. Res. Solid Earth. https://doi.org/10.1002/2016JB012972

Gutscher, M. A., Kopp, H., Krastel, S., Bohrmann, G., Garlan, T., Zaragosi, S., et al. (2017). Active tectonics of the Calabrian subduction revealed by new multi-beam bathymetric data and high-resolution seismic profiles in the Ionian Sea (Central Mediterranean). *Earth and Planetary Science Letters*. https://doi.org/10.1016/j.epsl.2016.12.020

Haji, T., Zouaghi, T., & Boukadi, N. (2014). The role of inherited structures in the evolution of the Meknassy Basin, Central Tunisia, based on geological-geophysical transects. *Journal of African Earth Sciences*. https://doi.org/10.1016/j.jafrearsci.2014.03.016

Henriquet, M., Dominguez, S., Barreca, G., Malavieille, J., Monaco, C., (2020). Structural and tectono-stratigraphic review of the Sicilian orogen and new insights from analogue modeling. Earth-Science Rev. https://doi.org/10.1016/j.earscirev.2020.103257

Hubbert, M. K. (1937). Theory of scale models as applied to the study of geologic structures. *Bulletin of the Geological Society of America*. https://doi.org/10.1130/GSAB-48-1459

Huw Davies, J., & von Blanckenburg, F. (1995). Slab breakoff: A model of lithosphere detachment and its test in the magmatism and deformation of collisional orogens. *Earth and Planetary Science Letters*, *129*(1–4), 85–102. https://doi.org/10.1016/0012-821X(94)00237-S

Jiménez-Munt, I., & Negredo, A. M. (2003). Neotectonic modelling of the western part of the Africa-Eurasia plate boundary: From the Mid-Atlantic ridge to Algeria. *Earth and Planetary Science Letters*. https://doi.org/10.1016/S0012-821X(02)01045-2

Jolivet, L., & Faccenna, C. (2000). Mediterranean extension and the Africa-Eurasia collision. *Tectonics*. https://doi.org/10.1029/2000TC900018

Kamoun, F., Peybernès, B., Ciszak, R., & Calzada, S. (2001). Triassic palaeogeography of Tunisia. *Palaeogeography, Palaeoclimatology, Palaeoecology*. https://doi.org/10.1016/S0031-0182(01)00283-8

Khelil, M., Souloumiac, P., Maillot, B., Khomsi, S., & Frizon de Lamotte, D. (2019). How to build an extensional basin in a contractional setting? Numerical and physical modelling applied to the Mejerda Basin at the front of the eastern Tell of Tunisia. *Journal of Structural Geology*. https://doi.org/10.1016/j.jsg.2019.103887

Khessibi, M., 1978. Etude géologique du secteur Maknassy-Mezzouna et du Jebel Kebar (Tunisie centrale). Thèse Univ. Claude Bernard, Lyon, 175p. (37 fig., 7pl.h.t).

Khomsi, S., Bédir, M., Zouari, H., & Ghazi Ben Jemia, M. (2004). Mise en évidence et analyse d'une structure atlasique ennoyée au front de la Chaîne alpine tunisienne. *Comptes Rendus Geoscience*. https://doi.org/10.1016/j.crte.2004.05.003

Khomsi, S., Ben Jemia, M. G., de Lamotte, D. F., Maherssi, C., Echihi, O., & Mezni, R. (2009). An overview of the Late Cretaceous-Eocene positive inversions and Oligo-Miocene subsidence events in the foreland of the Tunisian Atlas: Structural style and implications for the tectonic agenda of the Maghrebian Atlas system. *Tectonophysics*. https://doi.org/10.1016/j.tecto.2009.02.027

Khomsi, S., de Lamotte, D. F., Bédir, M., & Echihi, O. (2016). The Late Eocene and Late Miocene fronts of the Atlas Belt in eastern Maghreb: integration in the geodynamic evolution of the Mediterranean Domain. *Arabian Journal of Geosciences*. https://doi.org/10.1007/s12517-016-2609-1

Laaridhi-Ouazâa, N., 1994. Etude minéralogique et géochimique des épisodes magmatiques Mésozoïques et Miocènes de la Tunisie. PhD Es-Sciences thesis. University of Tunis II, 466 p. Published thesis

de Lamotte, D. F., Leturmy, P., Missenard, Y., Khomsi, S., Ruiz, G., Saddiqi, O., et al. (2009). Mesozoic and Cenozoic vertical movements in the Atlas system (Algeria, Morocco, Tunisia): An overview. *Tectonophysics*. https://doi.org/10.1016/j.tecto.2008.10.024

Lelandais, T., Mourgues, R., Ravier, É., Pochat, S., Strzerzynski, P., & Bourgeois, O. (2016). Experimental modeling of pressurized subglacial water flow: Implications for tunnel valley formation. *Journal of Geophysical Research: Earth Surface*, *121*(11), 2022–2041. https://doi.org/10.1002/2016JF003957

Leprêtre, R., De Lamotte, D. F., Combier, V., Gimeno-Vives, O., Mohn, G., & Eschard, R. (2018). The Tell-Rif orogenic system (Morocco, Algeria, Tunisia) and the structural heritage of the southern Tethys margin. *BSGF - Earth Sciences Bulletin*. https://doi.org/10.1051/bsgf/2018009

883 Lonergan, L., & White, N. (1997). Origin of the Betic-Rif mountain belt. *Tectonics*.
884 https://doi.org/10.1029/96TC03937Martinez and Truillet (1985). Evolution structurale et
885 paléogéographie de la Tunisie. Ment. Soc. Geol. It., 38 (1987), 35-45.

886 Masrouhi, A., Bellier, O., Ben Youssef, M., & Koyi, H. (2014). Submarine allochthonous salt sheets:
887 Gravity-driven deformation of North African Cretaceous passive margin in Tunisia - Bled Dogra
888 case study and nearby salt structures. *Journal of African Earth Sciences*.
889 https://doi.org/10.1016/j.jafrearsci.2014.04.032

890 Maury, R., Fourcade, S., Coulon, C., El Azzouzi, M., Bellon, H., Coutelle, A., et al. (2000). Post-
891 collisional Neogene magmatism of the Mediterranean Maghreb margin: A consequence of slab
892 breakoff. *Comptes Rendus de l'Academie de Sciences - Serie IIa: Sciences de La Terre et Des*
893 *Planetes*. https://doi.org/10.1016/S1251-8050(00)01406-3

894 Melki, F., Zouaghi, T., Ben, M., Bdir, M., & Zargouni, F. (2012). Role of the NE-SW Hercynian Master
895 Fault Systems and Associated Lineaments on the Structuring and Evolution of the Mesozoic and
896 Cenozoic Basins of the Alpine Margin, Northern Tunisia. In *Tectonics - Recent Advances*.
897 https://doi.org/10.5772/50145

898 Morgan, M. A., Grocott, J., & Moody, R. T. J. (1998). The structural evolution of the Zaghouan-Ressas
899 Structural Belt, northern Tunisia. *Geological Society Special Publication*.
900 https://doi.org/10.1144/GSL.SP.1998.132.01.23

901 Outtani, F., Addoum, B., Mercier, E., de Lamotte, D.F., Andrieux, J., (1995). Geometry and kinematics
902 of the South Atlas Front, Algeria and Tunisia. Tectonophysics. https://doi.org/10.1016/0040-
903 1951(95)00022-F

904 Patriat, M., Ellouz, N., Dey, Z., Gaulier, J. M., & Kilani Haten Ben, B. (2003). The Hammamet, Gabès
905 and Chotts basins (Tunisia): A review of the subsidence history. *Sedimentary Geology*.
906 https://doi.org/10.1016/S0037-0738(02)00290-7

907 Philip, H., Andrieux, J., Dlala, M., Chihi, L., & Ben Ayed, N. (1986). Evolution tectonique mio-
908 quaternaire du fosse de Kasserine (Tunisie centrale); implications sur l'evolution geodynamique
909 recente de la Tunisie. *Bulletin de La Société Géologique de France*.
910 https://doi.org/10.2113/gssgfbull.ii.4.559

911 Rabaute, A., Chamot-Rooke, N., 2014. Active Tectonics of Africa-Eurasia Boundary from Algiers to
912 Calabria. Map 1:1 500000ème, Paris, ISBN 978-2-9548197-0-9.

913 Ramberg, H. (1981). The role of gravity in orogenic belts. *Geological Society Special Publication*.
914 https://doi.org/10.1144/GSL.SP.1981.009.01.11

915 Rigane, A., & Gourmelen, C. (2011). Inverted intracontinental basin and vertical tectonics: The
916 Saharan Atlas in Tunisia. *Journal of African Earth Sciences*.
917 https://doi.org/10.1016/j.jafrearsci.2011.05.003

918 Roca, E. (2001). The Northwest Mediterranean Basin (Valencia Trough, Golf of Lions and Liguro-
919 Provençal basins): structure and geodynamic evolution. In *PeriTethys Memoir 6: Peri-Tethyan*
920 *Rift/Wrench Basins and Passive Margins.*

921 Rosenbaum, G., & Lister, G. S. (2004). Neogene and Quaternary rollback evolution of the Tyrrhenian
922 Sea, the Apennines, and the Sicilian Maghrebides. *Tectonics*.
923 https://doi.org/10.1029/2003TC001518

924 Roure, F., Casero, P., & Addoum, B. (2012). Alpine inversion of the North African margin and

delamination of its continental lithosphere. *Tectonics*. https://doi.org/10.1029/2011TC002989

Saïd, A., Chardon, D., Baby, P., & Ouali, J. (2011). Active oblique ramp faulting in the Southern Tunisian Atlas. *Tectonophysics*. https://doi.org/10.1016/j.tecto.2011.01.010

Serpelloni, E., Vannucci, G., Pondrelli, S., Argnani, A., Casula, G., Anzidei, M., et al. (2007). Kinematics of the Western Africa-Eurasia plate boundary from focal mechanisms and GPS data. *Geophysical Journal International*. https://doi.org/10.1111/j.1365-246X.2007.03367.x

Sokoutis, D., & Willingshofer, E. (2011). Decoupling during continental collision and intra-plate deformation. *Earth and Planetary Science Letters*. https://doi.org/10.1016/j.epsl.2011.03.028Soumaya, A., Ben Ayed, N., Delvaux, D., & Ghanmi, M. (2015). Spatial variation of present-day stress field and tectonic regime in Tunisia and surroundings from formal inversion of focal mechanisms: Geodynamic implications for central Mediterranean. *Tectonics*. https://doi.org/10.1002/2015TC003895

Souloumiac, P., Maillot, B., Leroy, Y.M., 2012. Bias due to side wall friction in sand box experiments. J. Struct. Geol. https://doi.org/10.1016/j.jsg.2011.11.002

Souquet, P., Peybernès, B., Saadi, J., Ben Youssef, M., Ghanmi, M., Zarbout, M., Chikhaoui, M., Kamoun, F., (1997). Séquences et cycles d'ordre 2 en régime extensif et transtensif : Exemple du Crétacé inférieur de l'Atlas tunisien. Bull. la Soc. Geol. Fr.

Soussi M (2000) Le Jurassique de la Tunisie Atlasique: Stratigraphie, Dynamique sédimentaire, Paléogéographie et Intérêt pétrolier. Unpublished thesis, Doctorat d'Etat, Université de Tunis El Manar II, Tunisie, 661 pp

Strzerzynski, P., Déverchère, J., Cattaneo, A., Domzig, A., Yelles, K., Mercier de Lépinay, B., et al. (2010). Tectonic inheritance and Pliocene-Pleistocene inversion of the Algerian margin around Algiers: Insights from multibeam and seismic reflection data. *Tectonics*. https://doi.org/10.1029/2009tc002547

Strzerzynski, P., Dominguez, S., Boudiaf, A., Déverchère, J., (2021). Tectonic Inversion and Geomorphic Evolution of the Algerian Margin Since Messinian Times: Insights From New Onshore/Offshore Analog Modeling Experiments. Tectonics. https://doi.org/10.1029/2020TC006369

Turki, M.M., 1985. Polycinématique et contrôle sédimentaire associé sur la cicatrice Zaghouan-Nebhana. Thèse ès-Sc., Univ. Tunis, Revue Sc. Terre, édit. INRST, Tunis, 1988, 262p.

The EGT'85 seismic experiment in Tunisia: a reconnaissance of the deep structures. (1992). *Tectonophysics*. https://doi.org/10.1016/0040-1951(92)90479-P

Van Hinsbergen, D. J. J., Vissers, R. L. M., & Spakman, W. (2014). Origin and consequences of western Mediterranean subduction, rollback, and slab segmentation. *Tectonics*. https://doi.org/10.1002/2013TC003349

Vannucci, G., Pondrelli, S., Argnani, A., Morelli, A., Gasperini, P., & Boschi, E. (2004). An atlas of mediterranean seismicity. *Annals of Geophysics*. https://doi.org/10.4401/ag-3276

White, D., Take, A., & Bolton, M. (2001). Measuring soil deformation in geotechnical models using digital images and PIV analysis. *10th International Conference on Computer Methods and Advances in Geomechanics*.

White, D. J., Take, W. A., & Bolton, M. D. (2003). Soil deformation measurement using particle image

966 velocimetry (PIV) and photogrammetry. *Geotechnique*.
967 https://doi.org/10.1680/geot.2003.53.7.619

968 Wildi, W. (1983). La chaîne tello-rifaine (Algérie, Maroc, Tunisie): Structure, stratigraphie et évolution
969 du Trias au Miocène. *Rev. Géogr. Phys. Géol. Dyn.*

970 Wortel, R., Govers, R., & Spakman, W. (2009). Continental Collision and the STEP-wise Evolution of
971 Convergent Plate Boundaries: From Structure to Dynamics. https://doi.org/10.1007/978-3-540-
972 87974-9_3

973 Zargouni, F. (1985). Tectonique de l'Atlas méridional de Tunisie, évolution géométrique et
974 cinématique des structures en zones de cisaillement. *Thèse d'Etat. Université Louis Pasteur,*
975 *Strasbourg, France*.

976 Zouaghi, T., Bédir, M., & Inoubli, M. H. (2005). 2D seismic interpretation of strike-slip faulting, salt
977 tectonics, and Cretaceous unconformities, Atlas Mountains, central Tunisia. *Journal of African*
978 *Earth Sciences*. https://doi.org/10.1016/j.jafrearsci.2005.09.010

979 Zouaghi, T., Ferhi, I., Bédir, M., Youssef, M. Ben, Gasmi, M., & Inoubli, M. H. (2011). Analysis of
980 Cretaceous (Aptian) strata in central Tunisia, using 2D seismic data and well logs. *Journal of*
981 *African Earth Sciences*. https://doi.org/10.1016/j.jafrearsci.2011.05.002

982